Constraints on Lorentz invariance and *CPT* violation using optical photometry and polarimetry of active galaxies BL Lacertae and S5 B0716+714

Andrew S. Friedman,* David Leon,† Kevin D. Crowley, Delwin Johnson, Grant Teply, David Tytler, and Brian G. Keating‡

Center for Astrophysics and Space Sciences, University of California, San Diego, La Jolla, California 92093, USA

Gary M. Cole§

Western Nevada College, Carson City, Nevada 89703, USA

(Received 24 September 2018; published 28 February 2019)

Various quantum gravity approaches that extend beyond the Standard Model predict Lorentz invariance and charge-parity-time violation at energies approaching the Planck scale. These models frequently predict a wavelength-dependent speed of light, which would result in time delays between promptly emitted photons at different energies, as well as a wavelength-dependent rotation of the plane of linear polarization for photons resulting from vacuum birefringence. Here, we describe a pilot program with an automated system of small telescopes that can simultaneously conduct high cadence optical photometry and polarimetry of active galactic nuclei (AGN) in multiple passbands. We use these observations as a proof of principle to demonstrate how such data can be used to test various Lorentz violation models, including special cases of the Standard Model extension (SME). In our initial campaign with this system, the Array Photo Polarimeter, we observed two AGN sources, including BL Lacertae at redshift $z = 0.069$, and S5 B0716 + 714 at $z = 0.31$. We demonstrate that optical polarimetry with a broadband *Luminance* filter combined with simultaneous I_c-band observations yields SME parameter constraints that are up to ∼10 and ∼30 times more sensitive than with a standard I_c-band filter, for SME models with mass dimension $d = 5$ and $d = 6$, respectively. Using only a small system of telescopes with an effective 0.45-m aperture, we further demonstrate $d = 5$ constraints for individual lines of sight that are within a factor of ∼1–10 in sensitivity to comparable constraints from optical polarimetry with a 3.6-m telescope. Such an approach could significantly improve existing SME constraints via a polarimetric all-sky survey of AGN with multiple 1-meter class telescopes.

DOI: 10.1103/PhysRevD.99.035045

I. INTRODUCTION

Special relativity and the Standard Model of particle physics obey the symmetry of Lorentz invariance, which has survived an enormous range of tests over the past century (see [1] for a review). However, many theoretical approaches seeking to unify quantum theory and general relativity predict that Lorentz invariance may be broken at energies approaching the Planck scale $E_p = \sqrt{c^5\hbar/G} = 1.22 \times 10^{19}$ GeV, perhaps due to the underlying quantized nature of spacetime (e.g., [2,3]). Since the relevant energies are not accessible to any current, or foreseeable, Earth-bound tests, most approaches to testing such models have relied on observations of high redshift astronomical sources to exploit small effects that may accumulate to detectable levels over cosmological distances and timescales.

This paper considers only Lorentz invariance violation (LIV) for photons,[1] which can lead to a modified vacuum dispersion relation and therefore an energy-dependent speed of light, which causes a time delay (or early arrival) for promptly emitted photons of different energies [5,13,14]. LIV models can also yield vacuum birefringence, which causes a rotation of the plane of linear polarization for promptly emitted photons at different energies emitted with the same initial polarization angle [13,15]. In general, each of these effects can be anisotropic, such that time delays and polarization rotations possess an

*asf@ucsd.edu
†dleon@physics.ucsd.edu
‡bkeating@ucsd.edu
§garycole@mac.com

[1]Other authors have considered testing LIV models for massive particles including neutrinos, which can be considered as approximately massless [3–7] and cosmic rays [8–12].

angular dependence on the sky and require observations of extended sources like the cosmic microwave background (CMB) or measurements of point sources along many lines of sight to fully test the LIV model parameter space [16,17].

Testing LIV is difficult because any relevant effects are expected to be negligible at energies accessible in Earth-bound or solar system experiments. However, any such effects could, in principle, accrue to measurable levels as these tiny deviations from Lorentz symmetry accumulate over cosmological distances. Qualitatively, evidence for LIV time delays from photometric observations are easier to measure for sources at higher cosmological redshifts and higher energies [4,5,13,16]. Compared to time delays, birefringent LIV models can be tested with much higher sensitivity using spectropolarimetry or broadband polarimetry [16].

In this work, we restrict our analysis to constraining a subset of the Standard Model extension (SME), an effective field theory approach describing the low energy corrections stemming from a more fundamental Planck scale theory of quantum gravity. The SME therefore provides a general framework for Lorentz invariance and charge-parity-time (CPT) violation tests with electromagnetic radiation [16].[2] More specifically, since we are only reporting observations of two optical AGN sources, we are limited to constraining either general SME models along specific lines of sight or vacuum isotropic SME models, which correspond to some of the more popular models studied in the literature. We further confine our analysis to SME models of mass operator dimension $d = 4$, 5, 6, 7, 8, 9. Mass dimension $d = 3$ models are best constrained with observations of the CMB [13,16,20–24].[3] While $d = 4$ models can yield birefringent effects, they would not produce LIV-induced time delays since they involve no changes to the usual photon dispersion relation [16].

Simultaneous photometric observations in two filters allows one to estimate upper limits to time delays between light curves in each bandpass. While our optical time delay constraints are not competitive with observations of gamma-ray bursts [9,27–43] or TeV flares from blazars [13,44–49], our approach, which may be unique in the literature, does constrain both time delays and maximum observed polarization with simultaneously obtained photometry and polarimetry using the same pair of broadband optical filters. As such, they have the promise to complement existing SME constraints.

Time delay measurements uniquely constrain the SME vacuum dispersion coefficients and, in principle, could constrain the vacuum birefringent coefficients as well for all models with $d \neq 4$. However, time delay measurements are typically less sensitive than broadband polarimetry for constraining the birefringent SME coefficients [16], so we exclusively use broadband polarimetry to constrain all other SME coefficients. While optical spectropolarimetry can yield constraints ∼2–3 orders of magnitude better for $d = 5$ models than broadband optical polarimetry [17], this generally requires $\gtrsim$2-meter class telescopes. With telescopes less than 1 m in diameter, broadband polarimetry in two or more filters is considerably more practical, offering a solution that is low cost and scalable to large numbers of observatories around the world. Since we did not obtain spectropolarimetry in our pilot program, we focus on the broadband polarimetry method for the rest of this work.

When observing a single source, as noted by [29], it is, in general, impossible to disentangle an intrinsic time lag at the source from a delay induced by genuine LIV dispersion effects.[4] Therefore, to constrain LIV models using observed time delays, one must either (A) assume that there are no intrinsic time delays or (B) statistically model observations of many sources using the fact that all LIV effects are predicted to increase with redshift and therefore be negligible for sufficiently "nearby" sources. For approach (B), one would model the population distribution of intrinsic time lags using a calibration sample of low redshift sources and then use this to disentangle these non-LIV effects from genuine LIV effects which could be manifest in a suitably matched population of higher redshift sources [16,17,29]. However, since we only observed one nearby source (BL Lacertae at $z = 0.0686 \pm 0.0004$ [52]) and one high redshift source (S5 B0716 + 714 at $z = 0.31 \pm 0.08$ [53,54]), we assume option (A) for the remainder of this work.

Similarly, it is, in general, impossible to know the intrinsic polarization angles for photons emitted with different energies from a given cosmological source. If one possessed this information, evidence for birefringence could be obtained by observing differences between the known intrinsic polarization angle and the actual observed angles for photons emitted promptly with the same polarization angle but at different energies. However, even in the absence of such knowledge, birefringent effects can be constrained for sources at arbitrary redshifts because a large degree of birefringence would yield large differences in observed polarization angles at nearby frequencies, effectively washing out most, if not all, of the observed polarization [16,37,42]. Therefore, observing a given polarization fraction can constrain wavelength-dependent birefringence effects, which, if in effect, would lead to a

[2]We therefore do not consider models such as doubly (or deformed) special relativity (e.g., [18,19]), which may not be compatible with the SME [16,17].

[3]For a discussion of the difficulties in calibrating the reference angle for astrophysical CMB polarization measurements, see [25,26].

[4]Note that the cosmological time delay calculation from [29] contains a basic error which was noted and corrected by [5] and used by subsequent analyses (e.g., [13,17]). This issue is also relevant for LIV tests using gravitational lensing [50] and pulsar timing [51].

smaller degree of observed polarization. To analyze SME models in this work, we follow the "average polarization" approach in [17].[5]

In this work, we present simultaneous photometric and polarimetric observations using two broadband optical filters on separate telescopes, including the *Luminance*-band filter (*Lum*) and a Johnson-Cousins I-band filter (I_c). While not as common as standard optical *BVRI* filters, we choose the wider *Lum* filter both to maximize the signal for our small telescopes and because wider optical bandpasses lead to tighter constraints on birefringent SME models obtained using any of the standard optical *BVRI* filters [17]. In particular, we demonstrate significant advantages of the wider *Lum* filter vs the narrower I_c filter, where, for the same observed maximum polarization fraction, the *Lum* filter yields $d = 5$, 6 SME parameter upper bounds that are factors of ∼3–26 times more sensitive than with the I_c-band filter.

In addition, we develop a technique to combine simultaneous polarimetric observations using two co-located telescopes with different filters into an effective system with a single broadband optical filter that avoids the expense of a half-wave plate with high transmission over the full ∼400–900-nm wavelength range of the combined $Lum + I_c$ filter. This yields more stringent SME constraints than either filter alone, while achieving the effective light collecting power of a larger telescope. This approach can be contrasted with an optical system using dichroic beam splitters on a single telescope to obtain simultaneous polarimetry in different bandpasses (e.g., the DIPOL-2 instrument [58]). With this approach, for the same observed maximum polarization fraction, our combined $Lum + I_c$ filter yields $d = 5$, 6 SME parameter upper bounds that are factors of ∼2–30 times more sensitive than with the I_c-band filter.

The pilot program in this work is meant as a proof of principle to obtain the most stringent SME constraints using broadband optical polarimetric observations with small telescopes for which spectropolarimetry is unfeasible. Even without spectropolarimetry, anisotropic SME constraints can be improved by observing sources along lines of sight without previously published optical polarimetry. Even if specific AGN sources have already published optical polarimetry, improved SME constraints can potentially be obtained simply by observing these sources with wider optical bandpasses and by potentially observing a larger maximum polarization value than previously found. For all of these reasons, this work aims to motivate design feasibility studies for a follow-up optical polarimetry survey using at least two 1-m class telescopes, with one or more in each hemisphere.

This paper is organized as follows. In Sec. II, we describe the Standard Model extension family of Lorentz and *CPT*-invariance violating models that we are interested in testing, and we present our main constraints. In Sec. III, we describe the optical polarimetric and photometric observing systems used in this work, with emphasis on correcting for systematic errors in our maximum polarization measurements. Conclusions are presented in Sec. IV. Mathematical details are presented in Appendix A and the data obtained for this paper are presented in Appendix B.

II. STANDARD MODEL EXTENSION

We do not describe the full SME framework here. Instead, see [16] for a review. Qualitatively, if the Standard Model holds perfectly, all SME coefficients vanish identically. No strong evidence yet exists for any nonzero SME coefficients, and therefore, many LIV models falling under the SME umbrella have already been ruled out. However, the general approach to make progress testing such models is to use observations of cosmological sources at different wavelengths, higher redshifts, and varied positions on the sky to progressively lower the upper bounds for any nonzero values of the coefficients over the full SME parameter space. Weak constraints imply very large, uninformative, upper bounds. Strong constraints imply very small, informative, upper bounds that constrain coefficient values progressively closer to zero. However, even seemingly weak constraints can be of value if they are obtained with an observational approach with smaller (or different) systematics than an approach that nominally yields stronger constraints [17].

A. Vacuum dispersion SME models

Most LIV models predict a wavelength-dependent speed of light, leading to light of a given energy arriving earlier (or later) than light of another energy, even if both were emitted simultaneously in the rest frame of the source. Following [5,13,16,37], using "natural" units (in which $\hbar = c = 1$), in the context of the SME, the arrival time difference between photons emitted simultaneously from a cosmological source with index label s at redshift $z = z_s$ and sky position (θ_s, ϕ_s), with observed energies E_1 and E_2 (detected at observer frame times t_1 and t_2, respectively), is given by

$$\Delta t^{(d)}_{(z_s)} = t_2 - t_1 \approx (E_2^{d-4} - E_1^{d-4}) L^{(d)}_{(z_s)} \sum_{jm} Y_{jm,s} c^{(d)}_{(I)jm}, \quad (1)$$

where $Y_{jm,s} \equiv Y_{jm}(\theta_s, \phi_s)$ are the spin weighted spherical harmonics for spin 0,[6] $c^{(d)}_{(I)jm}$ are the vacuum dispersion

[5]The authors in [17] also analyzed both optical polarimetry and spectropolarimetry, where available, from 72 existing polarized AGN and gamma-ray burst (GRB) afterglow sources in the literature (e.g., [55–57]).

[6]$Y_{jm} \equiv {}_0Y_{jm}$ are the usual spherical harmonics for spin 0.

SME coefficients with mass dimension $d = 4, 6, 8, \ldots$, which must be *CPT* even, and

$$L^{(d)}_{(z_s)} = \int_0^{z_s} \frac{(1+z)^{d-4}}{H(z)} dz = \int_{a_s}^{1} \frac{da}{(a)^{d-2} H(a)}, \quad (2)$$

where $L^{(d)}_{(z_s)}$ is the effective comoving distance traveled by the photons, including the cosmological effects needed to compute arrival time differences in an expanding universe [5]. Setting $d = 4$ recovers the usual expression for comoving distance. In Eq. (2), $H(z) = H(a)$ is the Hubble expansion rate at a redshift z_s with scale factor $a_s^{-1} = 1 + z_s$ [with the usual normalization $a(t_0) = 1$ at the present cosmic time $t = t_0$ at $z = 0$] given by

$$H(a) = H_0[\Omega_r a^{-4} + \Omega_m a^{-3} + \Omega_k a^{-2} + \Omega_\Lambda]^{1/2}, \quad (3)$$

in terms of the present-day Hubble constant, which we set to $H_0 = 73.24\ \mathrm{km\,s^{-1}\,Mpc^{-1}}$ [59], and best-fit cosmological parameters for matter $\Omega_m = 0.3089$, radiation $\Omega_r = \Omega_m/(1 + z_{eq}) = 9.16 \times 10^{-5}$ (with the matter-radiation equality redshift $z_{eq} = 3371$), vacuum energy $\Omega_\Lambda = 0.6911$, and curvature $\Omega_k = 1 - \Omega_r - \Omega_m - \Omega_\Lambda \approx 0$ using the Planck satellite 2015 data release [60].[7]

In principle, observations constraining the theoretical time delay $\Delta t^{(d)}_{(z_s)}$ from Eq. (1) between photons observed at different energies can constrain the SME coefficients $c^{(d)}_{(I)jm}$. More specifically, an upper bound $|\Delta t_\star|$ on the theoretical time delay (or early arrival) $|\Delta t^{(d)}_{(z_s)}| \leq |\Delta t_\star|$ measured from photometry in different bandpasses can be recast as an upper bound on a linear combination of SME coefficients:

$$|\bar{c}^{(d)}_{(I),s}| \lesssim \frac{c|\Delta t_\star|}{|E_2^{d-4} - E_1^{d-4}| L^{(d)}_{(z_s)}}, \quad (4)$$

where $\bar{c}^{(d)}_{(I),s} \equiv \sum_{jm} Y_{jm,s} c^{(d)}_{(I)jm}$ is shorthand for the linear combination of vacuum dispersion SME coefficients for source s and E_1 and E_2 can be estimated from the central wavelengths of the filters.

Figure 1 shows the relation between time delay upper limits and $d = 6$ isotropic SME models for sample sources observed with both our *Lum* and I_c filters over a range of redshifts $z \in [0.1, 1, 10]$, while highlighting the parameter space already ruled out by limits from GRB observations,

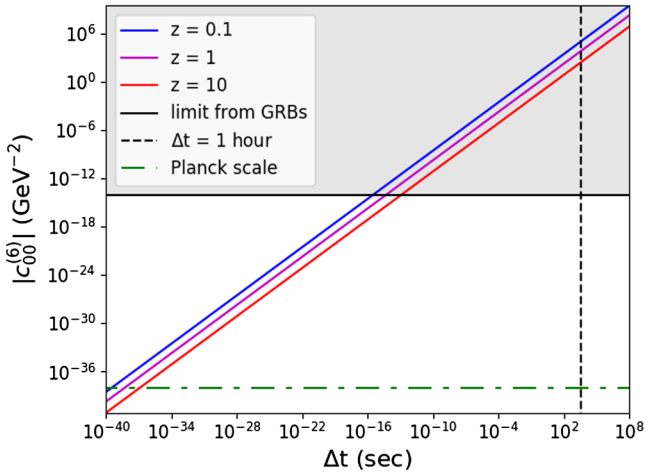

FIG. 1. We plot the dimension $d = 6$ isotropic vacuum dispersion SME parameter $|c^{(6)}_{(I)00}|$ for time delays between two example observations in the *Lum* and I_c bands (central wavelengths of ∼550 nm vs ∼800 nm) for various redshift sources ($z = 0.1$, 1, 10). The horizontal dot-dashed line shows the $|c^{(6)}_{(I)00}|$ corresponding to the Planck energy scale, while the dashed vertical line corresponds to a time delay of 1 hour. Gray regions in the parameter space with $|c^{(6)}_{(I)00}| \gtrsim 10^{-14}\ \mathrm{GeV}^{-2}$ have already been ruled out by high redshift, high time resolution, gamma-ray burst data [37]. Because of this, optical time delays on the order of minutes to hours for moderate redshift sources can only provide weak—but still independent—constraints as a consistency check.

as well as the weaker, but meaningful constraints obtainable from optical time delay data with $|\Delta t_\star| \leq 1$ hour.

B. *CPT*-odd vacuum birefringent SME models

For a subset of vacuum birefringent SME models with coefficients $k^{(d)}_{(V)jm}$, where the mass dimension $d = 3, 5, 7, \ldots$ must be *CPT* odd, rather than arrival times, the relevant quantity is the rotation of the plane of linear polarization for photons with different observed energies E_1 and E_2 that were emitted in the rest frame of the source with the same polarization angle. After traveling an effective distance of $L^{(d)}_{(z_s)}$ through an expanding universe, the difference in their observed polarization angles $\Delta\psi^{(d)}_{(z_s)} = \psi_2 - \psi_1$ will be

$$\Delta\psi^{(d)}_{(z_s)} \approx (E_2^{d-3} - E_1^{d-3}) L^{(d)}_{(z_s)} \sum_{jm} Y_{jm,s} k^{(d)}_{(V)jm}. \quad (5)$$

In principle, polarimetric observations measuring an observed polarization angle difference $|\Delta\psi_\star|$ in a single broadband filter with bandpass edge energies E_1 and E_2, with $|\Delta\psi^{(d)}_{(z_s)}| \leq |\Delta\psi_\star|$, can constrain the SME coefficients $k^{(d)}_{(V)jm}$ directly using Eq. (5),

[7]We use cosmological parameters reported in Table 4, column 6, of [60]. These are the joint cosmological constraints [TT, TE, EE + lowP + lensing + ext 68% limits (where ext = BAO + JLA + H0)]. However, based on recent tension between the Hubble constant H_0 determined using CMB data and type Ia supernovae (SN Ia), we use the SN Ia Hubble constant $H_0 = 73.24\ \mathrm{km\,s^{-1}\,Mpc^{-1}}$ [59] rather than $H_0 = 67.74\ \mathrm{km\,s^{-1}\,Mpc^{-1}}$ from Table 4, column 6, of [60].

$$|\bar{k}^{(d)}_{(V),s}| \leq \frac{c|\Delta\psi_\star|}{|E_2^{d-3} - E_1^{d-3}|L^{(d)}_{(z_s)}}, \quad (6)$$

where $\bar{k}^{(d)}_{(V),s} \equiv \sum_{jm} Y_{jm,s} k^{(d)}_{(V)jm}$ is shorthand for the linear combination of birefringent SME coefficients for source s.[8]

Equation (6) requires the assumption that all photons in the observed bandpass were emitted with the same (unknown) intrinsic polarization angle. When not making such an assumption, a more complicated and indirect argument is required. In general, when integrating over an energy range $[E_1, E_2]$, if LIV effects exist, the observed polarization degree will be substantially suppressed for a given observed energy if $\Delta\psi_\star > \pi$, regardless of the intrinsic polarization fraction at the corresponding rest frame energy [17,37]. Other authors present arguments allowing them to assume $\Delta\psi_\star \leq \pi/2$ to derive bounds on certain SME models [34–36]. In our case, observing a polarization fraction $p_\star$ can be used to constrain birefringent SME coefficients as follows.

First, one conservatively assumes a 100% intrinsic polarization fraction at the source for all wavelengths. Lower fractions for the source polarization spectrum would lead to tighter SME bounds. In this case, the total intensity I is equal to the polarized intensity I_p, such that

$$I = \int_{E_1}^{E_2} T(E)dE = I_p, \quad (7)$$

where $T(E)$ is the total throughput transmission function as a function of photon energy $E = hc/\lambda$ (with wavelength λ) for the polarimeter, including the relevant optics, broadband filters, and detectors (see Fig. 2). Then, following [17], integrating Eq. (5) over the energy range of the effective bandpass $T(E)$ yields normalized linear polarization Stokes parameters $q \equiv Q/I$ and $u \equiv U/I$, given by

$$\begin{aligned} q^{(d)}_{(z_s)} &= \frac{I_p}{I}\int_{E_1}^{E_2} \cos(2\Delta\psi)T(E)dE \\ &= \int_{E_1}^{E_2} \cos\left(2(E^{d-3} - E_1^{d-3})L^{(d)}_{(z_s)}\bar{k}^{(d)}_{(V),s}\right)T(E)dE, \end{aligned} \quad (8)$$

and

$$\begin{aligned} u^{(d)}_{(z_s)} &= \frac{I_p}{I}\int_{E_1}^{E_2} \sin(2\Delta\psi)T(E)dE \\ &= \int_{E_1}^{E_2} \sin\left(2(E^{d-3} - E_1^{d-3})L^{(d)}_{(z_s)}\bar{k}^{(d)}_{(V),s}\right)T(E)dE, \end{aligned} \quad (9)$$

[8]We present constraints from our data using the *Lum* and I_c-band optical filters in Sec. II E.

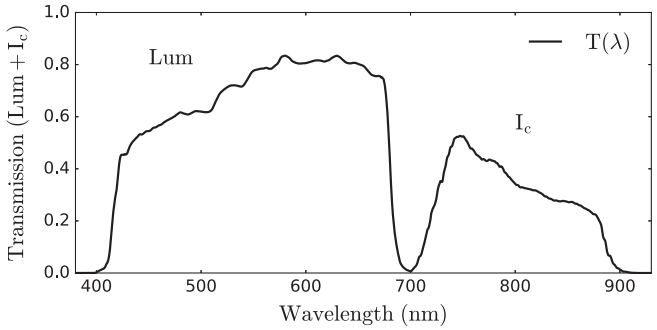

FIG. 2. Total transmission function from optics, filters, and CCD detectors for our *Lum* and I_c-bands observed using the Array Photo Polarimeter (APPOL, see Sec. III), which we combine into a single, effective broadband $Lum + I_c$ filter with coverage from ∼400–900 nm (with minimal filter overlap at ∼700 nm), using simultaneous data from two telescopes (see Fig. 8).

where the intensity normalized Stokes parameters $q = q^{(d)}_{(z_s)}$ and $u = u^{(d)}_{(z_s)}$ depend on mass dimension d and redshift z_s in the SME framework.

An upper bound on the observed polarization is then

$$p_\star - 2\sigma_\star < p^{(d)}_{\max,(z_s)} = \sqrt{(q^{(d)}_{(z_s)})^2 + (u^{(d)}_{(z_s)})^2}, \quad (10)$$

such that observing a polarization fraction $p_\star$ implies an upper bound on $\bar{k}^{(d)}_{(V),s}$ by finding the largest value of $\bar{k}^{(d)}_{(V),s}$ that is consistent with the inequality $p^{(d)}_{\max,(z_s)} > p_\star - 2\sigma_\star$, where $\sigma_\star$ is the $1-\sigma$ uncertainty on the polarization measurement. This corresponds to a 95% confidence interval assuming Gaussian measurement errors for the polarization fraction.

As shown by [17], in this framework, broader filters lead to smaller values for $p^{(d)}_{\max,(z_s)}$, so observing larger $p_\star$ values in those filters leads to tighter constraints on $\bar{k}^{(d)}_{(V),s}$ than observing the same polarization $p_\star$ through a narrower filter for the same source. In addition to improving our signal-to-noise ratio, this is a key reason we chose the broader *Lum* band filter to compare to the more standard I_c band filter and implemented a method to combine both filters using simultaneous observations on two telescopes. The transmission $T(\lambda)$ for our combined $Lum + I_c$-band polarimetry is shown in Fig. 2, which can be used to compute $T(E)$. Our observational setup is described in Sec. III.

In principle, one should also consider the source spectrum and the atmospheric attenuation in computing $T(E)$, but we follow [17] and assume that the optical spectra are flat enough in the relevant wavelength range so that we can ignore these small effects. However, unlike [17], which only considers the transmission function of the broadband filter, we additionally consider the transmission functions

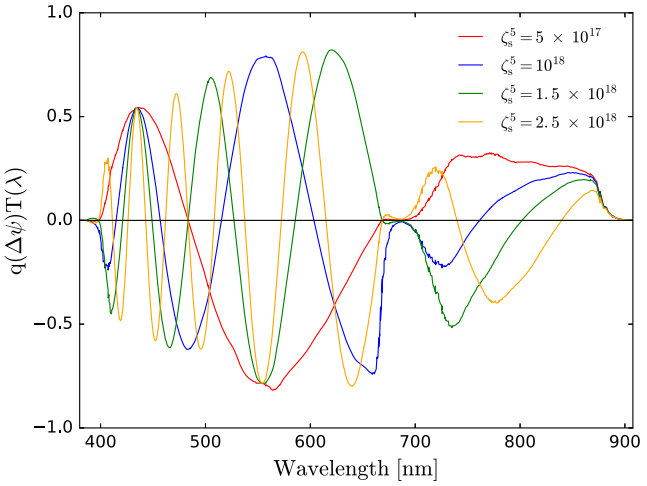

FIG. 3. Change of the Stokes parameter $q^{(d)}_{(z_s)}$ from Eq. (9) for our combined $Lum + I_c$ filter in Fig. 2 for several values of $\zeta_s^{(5)}$. For comparison, see Fig. 2 of [17].

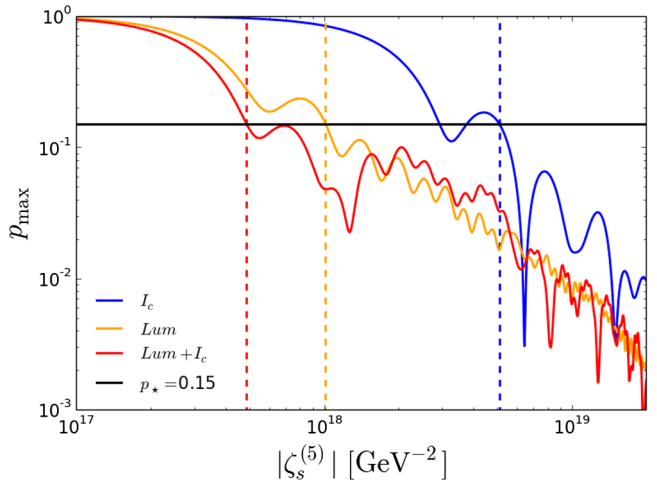

FIG. 4. Maximum allowed polarization fraction $p_{\max}$ vs $d = 5$ CPT-odd vacuum birefringence parameter $|\zeta_s^{(5)}|$ from Eq. (11) for the I_c band (blue), Lum band (orange), and our combined $Lum + I_c$ band (red). For an example observed polarization fraction $p_\star = 0.15$ (horizontal black line), upper limits on $|\zeta_s^{(5)}|$ for each band (dashed vertical lines) can be obtained by noting that $p_{\max}$ eventually falls below the observed value of $p_\star$ for all values of that coefficient. For $p_\star \gtrsim 0.02$, the most stringent upper limit comes from the combined $Lum + I_c$ band. For $p_\star = 0.15$, this yields a $Lum + I_c$-band upper limit $|\zeta_s^{(5)}| \lesssim 5.0 \times 10^{17}$ GeV^{-2}, a factor of ∼10 better than the corresponding limit from the I_c band.

for the optics and CCD detector, in addition to the filter, when computing $T(E)$ (see Fig. 8).

Following [17], to jointly parametrize the cosmological redshift dependence and SME parameter effects, we define the quantity $\zeta_s^{(5)}$ as

$$\zeta_s^{(5)} \equiv L^{(5)}_{(z_s)} \bar{k}^{(5)}_{(V),s}. \tag{11}$$

Also following [17], Fig. 3 shows the change in the intensity normalized Stokes parameter $q^{(d)}_{(z_s)}$ from Eq. (9) for several values of $\zeta_s^{(5)}$, while Fig. 4 shows theoretical limits from the maximum observed polarization $p_{\max}$ vs $|\zeta_s^{(5)}|$ in our Lum and I_c bands, and for our combined $Lum + I_c$ band in Fig. 2. Based on Fig. 4, Fig. 5 shows that the $Lum + I_c$ band yields $|\zeta_s^{(5)}|$ constraints ∼2–10 times more restrictive than the I_c band for the same observed polarization fraction, over the range $p_{\max} \gtrsim 0.02$ (where $p_\star < p_{\max}$), assuming negligible uncertainties, $\sigma_\star$.

C. *CPT*-odd vacuum isotropic SME models

Since jm are the angular quantum numbers with $-j \le m \le j$, with $j \le d-2$, for each value of d, the number of distinct anisotropic vacuum dispersion and vacuum birefringent SME coefficients increases as $(d-1)^2$ when d is CPT odd and as $3(d-1)^2 - 8$ when d is CPT even [16] (see Table II of [37]). For example, the $d = 5$ model has 16 SME coefficients [17]. Since we only observed two sources, we are limited to constraining only linear combinations of SME coefficients $c^{(d)}_{(I)jm}$ and $k^{(d)}_{(V)jm}$ along two specific lines of sight. Ultimately, progressively larger numbers of sources at different locations on the sky

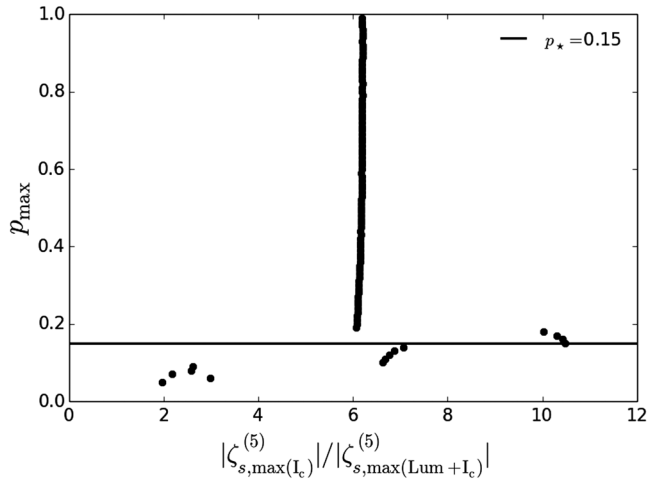

FIG. 5. Theoretical maximum observed polarization $p_{\max}$ vs the ratio of CPT-odd vacuum birefringent $d = 5$ SME coefficients from Fig. 4 from the I_c and $Lum + I_c$ bands, $|\zeta_s^{(5)}(I_c)|/|\zeta_s^{(5)}(Lum + I_c)|$. Ignoring polarization uncertainties $\sigma_\star$, for all observed polarization fractions $p_\star \gtrsim 0.02$ (where $p_\star < p_{\max}$), constraints from the $Lum + I_c$ band are ∼2–10 times tighter than for the I_c band. The spike at $|\zeta_s^{(5)}(I_c)|/|\zeta_s^{(5)}(Lum + I_c)| \sim 6$ results from the fact that the ratio of the $|\zeta_s^{(5)}|$ values in each band (blue and red curves in Fig. 4) is nearly constant for $p_\star \gtrsim 0.17$.

TABLE I. Celestial coordinates and *BVR* magnitudes of observed AGN sources from the Simbad database. *Lum* and I_c magnitudes are mean values from our own photometry in Tables V and VI.

	RA	DEC							
Name	IRCS (J2000)°	IRCS (J2000)°	Redshift z	z Ref.	B (mag)	V (mag)	R (mag)	*Lum* (mag)	I_c (mag)
S5 0716 + 714	110.47270192	+71.34343428	0.31 ± 0.08	[53,54]	15.50	14.17	14.27	14.65	14.10
BL Lacertae	330.68038079	+42.27777231	0.0686 ± 0.0004	[52]	15.66	14.72	13.00	13.89	13.06

are required to better constrain the general anisotropic model space for a given value of d.

However, we can follow a simpler approach and also test the subset of isotropic models, which are recovered for each value of d when setting $j = m = 0$. Lines of sight to individual point sources are therefore most useful for constraining the isotropic SME coefficients $c^{(d)}_{(I)00}$ and $k^{(d)}_{(V)00}$, which correspond to some of the simplest LIV models in the literature [16,37]. Constraints for both

TABLE II. Upper limits on linear combinations of SME coefficients of Lorentz and *CPT* violation along specific lines of sight from our *Lum* and I_c-band observations of BL Lacertae and S5 B0716 + 714, with sky coordinates and redshifts from Table I. The upper portion of the table shows the vacuum dispersion coefficients $|\bar{c}^{(d)}_{(I)}|$ and corresponding isotropic coefficients $|c^{(d)}_{(I)00}|$ (see Fig. 1) as inferred from estimates of an upper bound on the time delay $\Delta t_\star$ between the observed photometry in both the *Lum* and I_c bands as described in Sec. II E. The remaining rows show separate constraints from the maximum observed polarization fraction $p_\star$, which we correct for systematics from interstellar polarization ($p_{\mathrm{sys,ISP}}$) and instrumental polarization and zero point bias ($p_{\mathrm{sys,inst}}$), in each band via $p_{\star,\mathrm{cor}} = p_\star - p_{\mathrm{sys,ISP}} - p_{\mathrm{sys,inst}}$, with corresponding statistical errors added in quadrature. To be conservative, we derive SME parameter upper bounds using the $2-\sigma$ errors for $\Delta t_\star$, $p_{\star,\mathrm{cor}}$, and redshift z. The lower rows show the vacuum birefringent coefficients $|\bar{k}^{(d)}_{(V)}|$ and their corresponding isotropic coefficients $|k^{(d)}_{(V)00}|$, each for the *CPT*-odd cases $d = 5, 7, 9$. The last three rows show the vacuum birefringence coefficients $|\bar{k}^{(d)}_{(EB)}|$ for the *CPT*-even cases $d = 4, 6, 8$. In each case, constraints from our observed broadband polarimetry using the wider *Lum* band are tighter than for the I_c band.

Source	S5 B0716 + 714		BL Lacertae	
(RA, DEC)	(110.47°, 71.34°)		(330.68°, 42.28°)	
Redshift z	0.31 ± 0.08		0.0686 ± 0.0004	
Time delay upper bound	$I_c - Lum$		$I_c - Lum$	
$\lvert\Delta t_\star\rvert$ [minutes]	11.7		65.5	
$\lvert\bar{c}^{(6)}_{(I)}\rvert \equiv \lvert\sum_{jm} Y_{jm}(\theta,\phi) c^{(6)}_{(I)jm}\rvert$	$<6\times10^{+01}$ GeV^{-2}		$<8\times10^{+02}$ GeV^{-2}	
$\lvert\bar{c}^{(8)}_{(I)}\rvert \equiv \lvert\sum_{jm} Y_{jm}(\theta,\phi) c^{(8)}_{(I)jm}\rvert$	$<8\times10^{+18}$ GeV^{-4}		$<1\times10^{+20}$ GeV^{-4}	
$\lvert c^{(6)}_{(I)00}\rvert$	$<2\times10^{+02}$ GeV^{-2}		$<3\times10^{+03}$ GeV^{-2}	
$\lvert c^{(8)}_{(I)00}\rvert$	$<3\times10^{+19}$ GeV^{-4}		$<4\times10^{+20}$ GeV^{-4}	
Maximum observed polarization	*Lum*	I_c	*Lum*	I_c
$p_\star$ [%]	10.02 ± 0.44	8.30 ± 0.48	10.33 ± 0.43	10.50 ± 0.30
$p_{\mathrm{sys,ISP}}$ [%]	0.21 ± 0.27	0.77 ± 0.23	0.92 ± 0.07	0.46 ± 0.07
$p_{\mathrm{sys,int}}$ [%]	0.04	0.04	0.04	0.04
$p_{\star,\mathrm{cor}}$ [%]	9.77 ± 0.52	7.49 ± 0.53	9.37 ± 0.44	10.00 ± 0.31
$\lvert\bar{k}^{(5)}_{(V)}\rvert \equiv \lvert\sum_{jm} Y_{jm}(\theta,\phi) k^{(5)}_{(V)jm}\rvert$	$<1\times10^{-23}$ GeV^{-1}	$<7\times10^{-23}$ GeV^{-1}	$<3\times10^{-23}$ GeV^{-1}	$<1\times10^{-22}$ GeV^{-1}
$\lvert\bar{k}^{(7)}_{(V)}\rvert \equiv \lvert\sum_{jm} Y_{jm}(\theta,\phi) k^{(7)}_{(V)jm}\rvert$	$<2\times10^{-6}$ GeV^{-3}	$<1\times10^{-5}$ GeV^{-3}	$<4\times10^{-6}$ GeV^{-3}	$<2\times10^{-5}$ GeV^{-3}
$\lvert\bar{k}^{(9)}_{(V)}\rvert \equiv \lvert\sum_{jm} Y_{jm}(\theta,\phi) k^{(9)}_{(V)jm}\rvert$	$<3\times10^{+11}$ GeV^{-5}	$<4\times10^{+12}$ GeV^{-5}	$<8\times10^{+11}$ GeV^{-5}	$<6\times10^{+12}$ GeV^{-5}
$\lvert k^{(5)}_{(V)00}\rvert$	$<5\times10^{-23}$ GeV^{-1}	$<3\times10^{-22}$ GeV^{-1}	$<1\times10^{-22}$ GeV^{-1}	$<4\times10^{-22}$ GeV^{-1}
$\lvert k^{(7)}_{(V)00}\rvert$	$<6\times10^{-6}$ GeV^{-3}	$<3\times10^{-5}$ GeV^{-3}	$<2\times10^{-5}$ GeV^{-3}	$<8\times10^{-5}$ GeV^{-3}
$\lvert k^{(9)}_{(V)00}\rvert$	$<1\times10^{+12}$ GeV^{-5}	$<1\times10^{+13}$ GeV^{-5}	$<3\times10^{+12}$ GeV^{-5}	$<2\times10^{+13}$ GeV^{-5}
$\lvert\bar{k}^{(4)}_{(EB)}\rvert \equiv \lvert\sum_{jm\,2} Y_{jm}(\theta,\phi)(k^{(4)}_{(E)jm} + ik^{(4)}_{(B)jm})\rvert$	$\lesssim 7\times10^{-32}$	$\lesssim 2\times10^{-31}$	$\lesssim 2\times10^{-31}$	$\lesssim 3\times10^{-31}$
$\lvert\bar{k}^{(6)}_{(EB)}\rvert \equiv \lvert\sum_{jm\,2} Y_{jm}(\theta,\phi)(k^{(6)}_{(E)jm} + ik^{(6)}_{(B)jm})\rvert$	$\lesssim 5\times10^{-15}$ GeV^{-2}	$\lesssim 2\times10^{-14}$ GeV^{-2}	$\lesssim 1\times10^{-14}$ GeV^{-2}	$\lesssim 5\times10^{-14}$ GeV^{-2}
$\lvert\bar{k}^{(8)}_{(EB)}\rvert \equiv \lvert\sum_{jm\,2} Y_{jm}(\theta,\phi)(k^{(8)}_{(E)jm} + ik^{(8)}_{(B)jm})\rvert$	$\lesssim 2\times10^{+2}$ GeV^{-4}	$\lesssim 5\times10^{+3}$ GeV^{-4}	$\lesssim 4\times10^{+2}$ GeV^{-4}	$\lesssim 1\times10^{+4}$ GeV^{-4}

isotropic SME models and linear combinations along our specific lines of sight are shown in Table II.

D. *CPT*-even vacuum birefringent SME models

There exists an additional subset of *CPT*-even vacuum birefringent SME models with coefficients $k^{(d)}_{(E)jm}$ and $k^{(d)}_{(B)jm}$, where $d = 4, 6, 8, \ldots$, which correspond to spin-2 helicity, rather than spin 0. Let us first define

$$\bar{k}^{(d)}_{(EB),s} \equiv \sum_{jm} {}_{\pm 2}Y_{jm,s}\left(k^{(d)}_{(E)jm} + ik^{(d)}_{(B)jm}\right), \tag{12}$$

as shorthand for the linear combination of *CPT*-even birefringent SME coefficients for source s. Note that there are no isotropic models for this subset of SME parameters so there are no $jm = 00$ terms corresponding to Eq. (12) [16]. The *CPT*-even case is also more complex than the *CPT*-odd case, because the normal modes are linearly polarized and, in general, can involve no change in the polarization angle, or mixing of linearly polarized into elliptical or circularly polarized modes [37].

Following [16,37], we now define the accumulated phase change Φ at a given energy E as

$$\Phi_s = 2E^{d-3}L^{(d)}_{(z_s)}\bar{k}^{(d)}_{(EB),s}. \tag{13}$$

In the *CPT*-odd vacuum birefringent case, this phase change directly results in a polarization angle rotation because we can split linearly polarized light equally into left and right circularly polarized states. But the same is not true of the *CPT*-even case. Linearly polarized light will not, in general, be split evenly between the normal modes of a *CPT*-even Lorentz violation.

But similar to the *CPT*-odd case, we can still arrive at an expression for the maximum allowed polarization given a particular broadband filter. Again assuming a 100% polarized source at all wavelengths, the observation of a linear polarization fraction $p_\star$ (with uncertainty $\sigma_\star$) in a given broad energy band can be used to constrain the quantity $\bar{k}^{(d)}_{(EB),s}$.

Following [37], let us first define the angle $\Psi = \psi_0 - \psi_b$ as the difference between the initial polarization angle ψ_0 for light not produced in a normal mode and the initial polarization angle ψ_b for the slower of the two normal modes. For simplicity, we omit the source index s from the notation for Ψ, ψ_0, and ψ_b, since we will soon make assumptions which remove the Ψ dependence.

Additionally, we can define $\langle\cos\Phi_s\rangle$ as the average value of $\cos\Phi_s$ for source s after integrating over the relevant energy band

$$\langle\cos\Phi_s\rangle \equiv \int_{E_1}^{E_2} \cos(2(E^{d-3} - E_1^{d-3})L^{(d)}_{(z_s)}\bar{k}^{(d)}_{(EB),s})T(E)dE. \tag{14}$$

In this case, as shown in Appendix A, the normalized Stokes parameters $q = q^{(d)}_{(z_s)}$ and $u = u^{(d)}_{(z_s)}$ are

$$q^{(d)}_{(z_s)} = \cos 2\Psi \cos 2\psi_b - \langle\cos\Phi_s\rangle^2 \sin 2\Psi \sin 2\psi_b, \tag{15}$$

$$u^{(d)}_{(z_s)} = \cos 2\Psi \sin 2\psi_b + \langle\cos\Phi_s\rangle^2 \sin 2\Psi \cos 2\psi_b, \tag{16}$$

and, via Eq. (10), the corresponding maximum limit on polarization is

$$p_\star - 2\sigma_\star < p^{(d)}_{\max,(z_s)} = \sqrt{1 - (1 - \langle\cos\Phi_s\rangle^2)\sin^2 2\Psi} \leq |\langle\cos\Phi_s\rangle|, \tag{17}$$

where the conservative upper bound is reached when $\Psi = \pi/4$. Figure 6 shows the corresponding limits obtained in this most conservative case.

Similar to Fig. 4, Fig. 6 shows limits from the theoretical maximum polarization $p_{\max}$ in our *Lum*, I_c, and *Lum* + I_c bands vs the quantity $\zeta^{(6)}_s$, defined as

$$\zeta^{(6)}_s \equiv L^{(6)}_{(z_s)}\bar{k}^{(6)}_{(EB),s}. \tag{18}$$

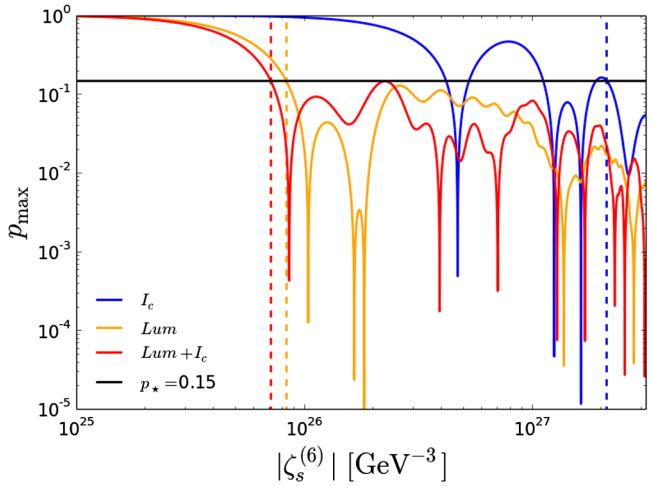

FIG. 6. Similar to Fig. 4, but for $p_{\max}$ vs the $d = 6$ *CPT*-even vacuum birefringence parameter $|\zeta^{(6)}_s|$ from Eq. (18). For an example observed polarization fraction $p_\star = 0.15$ (horizontal black line), the most stringent upper limit of $|\zeta^{(6)}_s| \lesssim 7 \times 10^{25}$ GeV^{-3} (dashed red line) comes from our combined *Lum* + I_c band, a factor of ~30 better than the corresponding limit from the I_c band (dashed blue line).

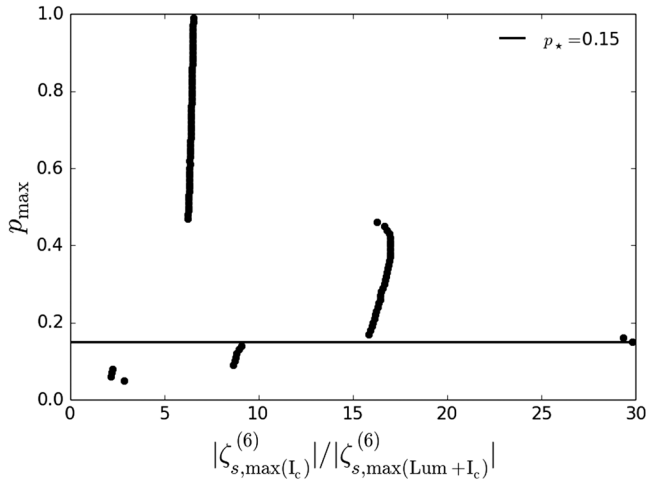

FIG. 7. Similar to Fig. 5, but for $p_{\max}$ vs the ratio of *CPT*-even vacuum birefringent $d = 6$ SME coefficients from Fig. 6 from the I_c and $Lum + I_c$ bands, $|\zeta^{(6)}_s(I_c)|/|\zeta^{(6)}_s(Lum + I_c)|$. Again, ignoring polarization uncertainties $\sigma_\star$, for all observed polarization fractions $p_\star \gtrsim 0.1$ and for many values $p_\star < 0.1$ (where $p_\star < p_{\max}$), constraints from the $Lum + I_c$ band are ∼3–30 times tighter than for the I_c band.

Again, similar to Figs. 5 and 7 shows that the combined $Lum + I_c$ band yields $|\zeta^{(6)}_s|$ constraints up to ∼3–30 times more sensitive than the I_c band.

E. Constraints on SME models

With simultaneous photometric time series in two filter bands, one can estimate upper limits to any time delays (or early arrivals) between the corresponding light curves under the simple assumption that the intrinsic light curve shapes are identical. We perform this analysis on our entire photometric time series (see Tables V and VI and Figs. 9–13) using an open source implementation of the discrete correlation function (DCF) in Python,[9] which can be used to analyze variable time series with arbitrary sampling [61] (see, e.g., [62]). Constraints from time delays are presented in Table II, using the methods of Sec. II A.

We consider possible estimated time delays $\Delta t_\star = m_L - m_I$ between observed photometric light curves in the *Lum* and I_c bands. Since our data points have a typical 8–10-minute cadence, we compute the best-fit DCF time delay using a series of DCF bin widths in the range [5, 20] minutes with step size 0.1 minutes, while considering possible time delays or early arrivals in the range of $[-250, 250]$ minutes for both sources. The mean and standard deviation of the set of best-fit DCF time delays then yield $\Delta t_\star = 26.5 \pm 19.5$ minutes and $\Delta t_\star = -5.1 \pm 3.3$ minutes for BL Lacertae and S5 B0716 + 714, respectively. Both are consistent with $\Delta t_\star = 0$, and thus no time delay, to within the $2-\sigma$ uncertainties. Using the $2-\sigma$ errors, and remaining agnostic as to the sign of $\Delta t^{(d)}_{(z_s)}$, leads to conservative time delay upper bounds of

$$|\Delta t_\star| \leq \max\{|\Delta t_\star - 2\sigma_{\Delta t_\star}|, |\Delta t_\star + 2\sigma_{\Delta t_\star}|\}, \quad (19)$$

which for the two sources yields $|\Delta t^{(d)}_{(z_s)}| \leq |\Delta t_\star| = 65.5$ minutes and 11.7 minutes, for BL Lacertae and S5 B0716 + 714, respectively.[10]

For a polarimetric time series measuring the polarization p in either the *Lum*, I_c, or combined $Lum + I_c$ bands, one can use the maximum observed polarization $p_\star$ during the observing period to place limits on the SME parameters as in Secs. II B–II D, with an additional correction for systematic errors described in Sec. III A. While a longer survey could, in principle, yield larger values of $p_\star$, and thus, more stringent SME constraints, meaningful constraints can still be obtained for arbitrary values of $p_\star$, even though these are likely lower limits to the true maximum polarization. Constraints from maximum observed polarization measurements are presented in Table II for the *Lum* and I_c bands, and in Table III for the combined $Lum + I_c$ band.

Even though we observed only two low redshift sources with small telescopes, our best *Lum*-band $d = 5$ SME constraint from maximum polarization measurements of S5 B0716 + 714 at $z = 0.31 \pm 0.08$ in Tables II and III of $|\bar{k}^{(5)}_{(V)}| < 1 \times 10^{-23}$ GeV^{-1} is within an order of magnitude of all constraints for individual lines of sight from the 36 QSOs in the redshift range $z \in [0.634, 2.936]$ analyzed in Table II of [17], where their SME parameter $\gamma_{\max}$ corresponds to our parameter $|\bar{k}^{(5)}_{(V)}|$.[11] More specifically, our best $d = 5$ constraint is comparable to the least sensitive constraint $\gamma_{\max} < 9.79 \times 10^{-24}$ GeV^{-1} from Table II of [17] (for FIRST J21079-0620 with $p_\star = 1.12 \pm 0.22\%$ at $z = 0.644$), while our best constraint is only a factor of ∼10 less sensitive than the *best* constraint of $\gamma_{\max} < 0.97 \times 10^{-24}$ GeV^{-1} (for PKS 1256 229 with $p_\star = 22.32 \pm 0.15\%$ at $z = 1.365$). This is the case even though our analysis was arguably more conservative than [17], in regards to modeling our transmission functions, correcting for polarimetry systematics, and including uncertainties in the reported redshift measurements.

Note that the sources analyzed in [17] used linear polarization measurements from [56], which were observed

[9] https://github.com/astronomerdamo/pydcf.

[10] The time delay upper limit for BL Lacertae is less stringent than the limit for S5 B0716 + 714 due mainly to the smaller number of data points.

[11] Our $Lum + I_c$, $\bar{k}^{(5)}_{(V)}$ constraint is actually a factor of ∼2 worse than our *Lum*-band constraint because the maximum observed polarization for the combined $Lum + I_c$ band data of $p_{\star,\mathrm{cor}} = 7.83 \pm 0.38\%$ is slightly smaller than the *Lum* band measurement of $p_{\star,\mathrm{cor}} = 9.77 \pm 0.52\%$. However, for the same value of $p_{\star,\mathrm{cor}}$, the $Lum + Ic$ constraint will always be more sensitive than the *Lum* or I_c-band constraints alone.

TABLE III. Same as SME coefficient limits from maximum observed polarization from Table II, but for the combined $Lum + I_c$ band (see Fig. 2).

Source	S5 B0716 + 714	BL Lacertae
(*RA*, *DEC*)	(110.47°, 71.34°)	(330.68°, 42.28°)
Redshift z	0.31 ± 0.08	0.0686 ± 0.0004
Maximum observed polarization	$Lum + I_c$	$Lum + I_c$
$p_\star$ [%]	8.64 ± 0.30	10.30 ± 0.28
$p_{\mathrm{sys,ISP}}$ [%]	0.77 ± 0.23	0.92 ± 0.07
$p_{\mathrm{sys,inst}}$ [%]	0.04	0.04
$p_{\star,\mathrm{cor}}$ [%]	7.83 ± 0.38	9.34 ± 0.29
$\lvert\tilde{k}^{(5)}_{(V)}\rvert \equiv \lvert\sum_{jm} Y_{jm}(\theta,\phi) k^{(5)}_{(V)jm}\rvert$	$<2 \times 10^{-23}$ GeV^{-1}	$<5 \times 10^{-23}$ GeV^{-1}
$\lvert\tilde{k}^{(7)}_{(V)}\rvert \equiv \lvert\sum_{jm} Y_{jm}(\theta,\phi) k^{(7)}_{(V)jm}\rvert$	$<4 \times 10^{-6}$ GeV^{-3}	$<8 \times 10^{-6}$ GeV^{-3}
$\lvert\tilde{k}^{(9)}_{(V)}\rvert \equiv \lvert\sum_{jm} Y_{jm}(\theta,\phi) k^{(9)}_{(V)jm}\rvert$	$<8 \times 10^{+11}$ GeV^{-5}	$<2 \times 10^{+12}$ GeV^{-5}
$\lvert k^{(5)}_{(V)00}\rvert$	$<9 \times 10^{-23}$ GeV^{-1}	$<2 \times 10^{-22}$ GeV^{-1}
$\lvert k^{(7)}_{(V)00}\rvert$	$<1 \times 10^{-5}$ GeV^{-3}	$<3 \times 10^{-5}$ GeV^{-3}
$\lvert k^{(9)}_{(V)00}\rvert$	$<3 \times 10^{+12}$ GeV^{-5}	$<7 \times 10^{+12}$ GeV^{-5}
$\lvert\tilde{k}^{(4)}_{(EB)}\rvert \equiv \lvert\sum_{jm\ 2} Y_{jm}(\theta,\phi)(k^{(4)}_{(E)jm} + ik^{(4)}_{(B)jm})\rvert$	$\lesssim 8 \times 10^{-32}$	$\lesssim 2 \times 10^{-31}$
$\lvert\tilde{k}^{(6)}_{(EB)}\rvert \equiv \lvert\sum_{jm\ 2} Y_{jm}(\theta,\phi)(k^{(6)}_{(E)jm} + ik^{(6)}_{(B)jm})\rvert$	$\lesssim 9 \times 10^{-15}$ GeV^{-2}	$\lesssim 5 \times 10^{-15}$ GeV^{-2}
$\lvert\tilde{k}^{(8)}_{(EB)}\rvert \equiv \lvert\sum_{jm\ 2} Y_{jm}(\theta,\phi)(k^{(8)}_{(E)jm} + ik^{(8)}_{(B)jm})\rvert$	$\lesssim 2 \times 10^{+2}$ GeV^{-4}	$\lesssim 4 \times 10^{+2}$ GeV^{-4}

using the 3.6-m telescope at the European Southern Observatory in La Silla, with the EFOSC2 polarimeter equipped with a V-band filter. As such, this work demonstrates that meaningful SME constraints for individual lines of sight—that are comparable to, or within a factor of 10 as sensitive as polarimetry constraints from a 3.6-m telescope—can be readily obtained using a polarimetric $Lum + I_c$-band system of small telescopes with an effective 0.45-m aperture, with ∼64 times less collecting area, which we describe in Sec. III.

III. THE ARRAY PHOTO POLARIMETER

The observing system used in this work, the Array Photo Polarimeter (APPOL)—maintained and operated by one of us (G. C.)—uses dual beam inversion optical polarimetry with Savart plate analyzers rotated through an image sequence with various half-wave-plate (HWP) positions. See [64–66] for the basic procedures underlying dual beam polarimetry. This approach can be contrasted with quadruple beam analyzers with Wollaston prisms such as RoboPol (e.g., [67–69]) that can obtain all the Stokes parameters in a suitably calibrated single image.

The APPOL array employs an automated telescope, filter, and instrument control system with 5 co-located telescopes on two mounts. APPOL uses two small, Celestron 11 and 14 inch, primary telescopes (C11 and C14) for polarimetry with an effective collecting area equivalent to a larger 17.8-inch (0.45-m) telescope, with added capability to obtain simultaneous photometry or polarimetry on a third smaller telescope (Celestron 8 inch = C8), along with bright star photometry and/or guiding using a fourth and fifth 5-inch telescope. APPOL is located at StarPhysics Observatory (Reno, Nevada) at an elevation of 1585 meters.

Earlier iterations of APPOL (e.g., [70]) have been progressively equipped with new automated instrumentation and image reduction software [71–73], and used for spectropolarimetry studies [74,75], including a long observing campaign presenting polarimetry and photometry of the variable star Epsilon Aurigae [76–78]. APPOL's polarimeter designs also helped inform the planning and hardware implementation of the University of Denver's DUSTPol instrument, an optical polarimeter with low instrumental polarization that has been used to study cool star systems, including RS CVn systems and Wolf-Rayet stars [79].

The first row of Fig. 8 shows the inputs to the total transmission vs wavelength $T(\lambda)$ in Fig. 2 for our *Lum* and I_c-band polarimetry using APPOL, which can be used to compute $T(E)$ as in Secs. II B–II E. The APPOL setup used in this work and the associated polarimetry data reduction and analysis methods will be described in more detail in a companion paper [80].

A. Observations and systematics

All data in this paper were observed with APPOL over a short campaign from December 2017 to January 2018. Samples of the observed data for BL Lacertae and S5

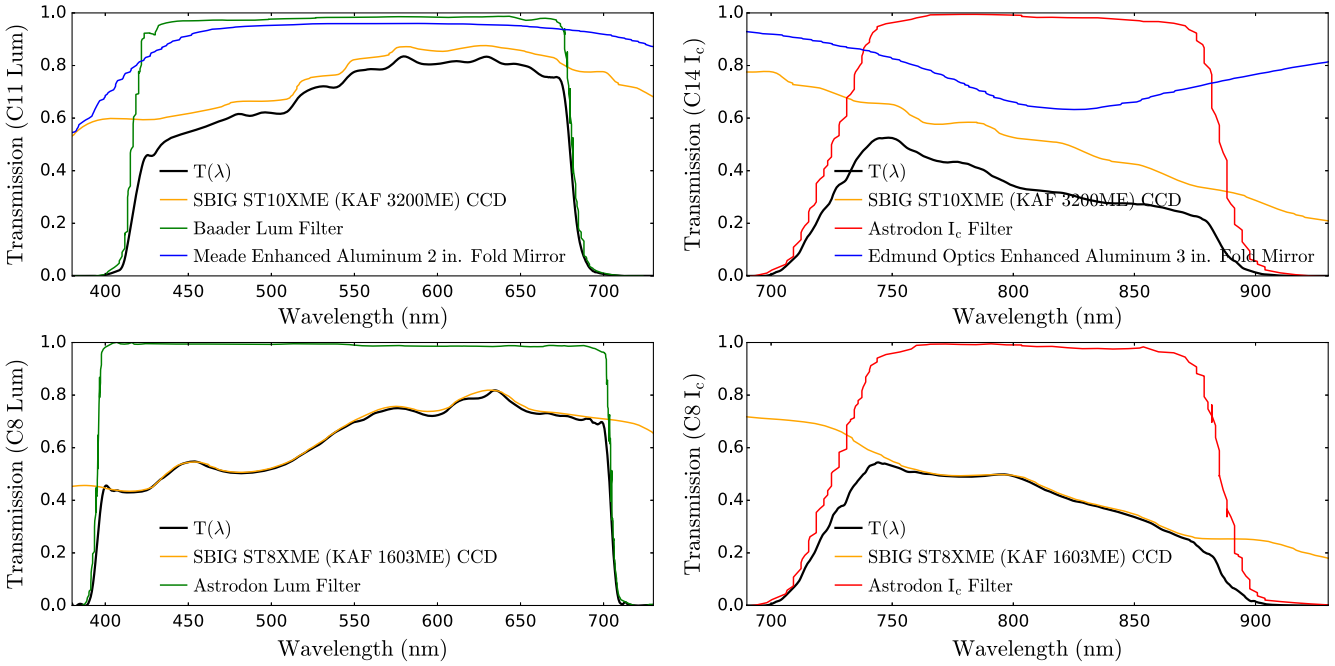

FIG. 8. Array photo polarimeter transmission functions for the relevant optical components, filters, and CCD detectors. The first row shows the C11 and C14 telescopes used for polarimetry in the *Lum* and I_c bands, respectively. The second row shows the C8 telescope used for photometry in both the I_c and *Lum* bands. The black curve shows $T(\lambda)$, the total transmission function, which can be used to compute $T(E)$ to constrain the SME parameters via maximum polarization measurements as in Secs. II B–II E. To simplify the analysis, we do not model the transmission functions of the Celestron StarBright coatings. We do not model the transmission functions of either the Savart Plates or the half-wave plates, which are fairly uniform throughout the relevant wavelength range. For similar reasons, we also neglect the atmospheric transmission and the source spectra. By comparison, the analysis in [17] only included the filter transmission function.

B0716 + 714 are shown in Appendix B in Tables V and VI, with the full machine-readable polarimetry and photometry data available at [63] and plotted in Figs. 9–11 for BL Lacertae and in Figs. 12–14 for S5 B0716 + 714. Image sequences with detected cosmic rays were identified as outliers and excluded. While we only use the maximum observed polarization to constrain birefringent SME models, we include the entire time series for completeness. By contrast, the full photometric time series was used to constrain the vacuum dispersion SME models using estimated time delays.

Optical photometric and polarimetric variability, correlations between flux and color, and searches for intraband photometric time lags have been studied extensively in the literature for AGN and BL Lacertae type objects [56,81–85], including the specific, well-known AGN sources we observed: BL Lacertae [86–89] and S5 B0716 + 714 [90–98]. Our analysis is restricted to testing SME models, but our photometric and polarimetric time series could be analyzed similarly in future work.[12]

Our data reduction pipeline removes systematic instrumental polarization using secondary flat-field self-calibration from the two sets of images taken at the 4 half-wave-plate positions (0°, 22.5°) and (45°, 67.5°), respectively, following [66]. Hundreds of previous APPOL measurements of unpolarized standard stars indicate that this procedure yields instrumental polarization systematics $\lesssim$0.03% for targets with sufficient flux, while zero-point bias adjustments are typically $\lesssim$0.01% for observed APPOL polarization fractions of greater than a few percent [77].[13] The APPOL HWP wave plate modulation efficiencies have been measured to be $\gtrsim$97% and ∼90% for *Lum* and I_c, respectively. Since imperfect modulation efficiency can only reduce the maximum observed polarization from its true value, to be conservative, we choose not to model these systematics here.[14] Previous tests indicate that other potential systematics including coordinate frame misalignment are negligible for APPOL [77].

The total optical polarization along arbitrary lines of sight toward galactic field stars can range from a fraction of a percent to several percent [105–107]. Previous work from

[12]For reviews of the many other applications of optical polarimetry, see, e.g., [99–104].

[13]We assume the same systematic error budget of 0.04% for the *Lum*, I_c, and *Lum* + I_c bands including instrumental polarization and zero-point bias.

[14]HWP modulation efficiency systematics would not affect the measured polarization angles, although other relevant systematics are discussed in [77].

TABLE IV. Polarization measurements p_L (*Lum*) and p_I (I_c) of field stars in sample image sequences within 3 arcmin of the AGN sources BL Lacertae and S5 B0716 + 714, used to estimate upper limits on interstellar polarization for the systematic error budget used in Tables II and III. Celestial coordinates and GAIA DR2 identifiers from Simbad/VizieR are included.

		RA	DEC		
Star #	GAIA DR2 ID	IRCS (J2000)°	IRCS (J2000)°	p_L (%)	p_I (%)
		BL Lacertae			
1	1960066324769508992	330.68924090	+42.27652024	1.01 ± 0.03	0.55 ± 0.03
2	1960066329068001536	330.69304715	+42.28231354	0.92 ± 0.07	0.46 ± 0.07
		S5 B0716 + 714			
1	1111278261916148224	110.47651216	+71.32247695	0.26 ± 0.43	0.89 ± 0.73
2	1111278158836933888	110.46803636	+71.30492029	0.21 ± 0.27	0.77 ± 0.23

the Large Interstellar Polarization Survey provided evidence that interstellar polarization (ISP) from multiple dust clouds along a given line of sight is smaller than from lines of sight passing through a single dust cloud [107,108]. Since the presence of two or more clouds would therefore depolarize the incoming radiation, we assume that the ISP along the line of sight toward a galactic field star represents a conservative upper limit to the true ISP toward an AGN source that would have been measured through the full dust column of the galaxy, the intergalactic medium, and the AGN host galaxy.

Using a sample image sequence for each of our two AGN targets, we performed *Lum* and I_c-band polarimetry on the two closest field stars within 3 arcmin of the target AGN, finding polarizations of $1.01 \pm 0.03\%$ and $0.92 \pm 0.07\%$ in *Lum* and $0.55 \pm 0.03\%$ and $0.46 \pm 0.07\%$ in I_c for the field of BL Lacertae and $0.26 \pm 0.43\%$ and $0.21 \pm 0.27\%$ in *Lum* and $0.89 \pm 0.73\%$ and $0.77 \pm 0.23\%$ in I_c for the field of S5 B0716 + 714. See Table IV. For the combined $Lum + I_c$ band maximum polarization measurements, we use the largest ISP measurement from the *Lum* and I_c bands.

Assuming that our AGN max polarization measurements arise from a combination of instrumental polarization, zero-point bias, ISP, and intrinsic source polarization, and that the ISP is approximately constant within 3 arcmin of the AGN target line of sight, we use the smaller of the two measured stellar polarizations to estimate conservative systematic upper limits for ISP ($p_{\mathrm{sys,ISP}}$) as listed in Tables II and III. Finally, to obtain a polarization estimate corrected for systematics, $p_{\star,cor}$, we subtract these systematic error estimates for ISP ($p_{\mathrm{sys,ISP}}$) as well as the 0.04% systematic budget from instrumental polarization and zero-point bias ($p_{\mathrm{sys,inst}}$) from our maximum observed polarization in the I_c, *Lum*, and $Lum + I_c$ bands to obtain the SME constraints in Tables II and III.[15]

[15]Statistical errors from the polarization measurements for the AGN source and stars used to estimate ISP systematics are added in quadrature.

IV. CONCLUSIONS

In this work, we performed optical polarimetry and photometry of two well-known AGN sources, BL Lacertae and S5 B0716 + 714 in both the *Lum* and I_c bands, while implementing a procedure to obtain polarimetry in a wider effective passband with coverage from ~400 to 900 nm by combining simultaneous photometry from two small, co-located telescopes. We used the "average polarization" method of [17], which analyzed polarimetric measurements from the literature, to analyze our own polarimetric measurements, thereby demonstrating a proof-of-principle method to use our own data to derive meaningful constraints, for individual lines of sight or isotropic models, on parameters from various subsets of the Standard Model extension, a useful framework to test for new physics beyond the Standard Model, including potential violation of Lorentz and *CPT* invariance [16]. We demonstrated that maximum polarization measurements with our wider effective $Lum + I_c$ bandpass can yield SME constraints that are up to ~10 or ~30 times more sensitive than with our I_c-band filter, for $d = 5$ and $d = 6$ models, respectively.

To constrain SME parameters for a single source along a single line of sight, optical photometric measurements of AGN are not competitive with GRB gamma-ray and x-ray measurements in regards to timing resolution, energy, and redshift. Therefore, high energy GRB measurements are the best way to constrain SME parameters using observed time delays at different observed energies. Nevertheless, GRBs are transients both in their prompt gamma-ray emission and optical afterglows. Therefore, since AGN are the brightest continuous optical sources at cosmological distances, it is considerably easier to quickly obtain more complete sky coverage by observing many more AGN, in order to better constrain the anisotropic vacuum dispersion SME models. In addition, compared with gamma- and x-ray polarimetry, optical polarimetric measurements typically have smaller statistical uncertainties and independent systematics [17]. Optical polarimetry is also easier to

obtain with ground-based instruments than gamma-ray and x-ray polarimetry, which must be obtained from space (e.g., [36]).

Although the limits presented here were not intended to compete with other approaches using maximum polarization measurements integrated over an optical bandpass, the pilot program in this work nevertheless demonstrates that meaningful SME constraints can be obtained even with a small set of telescopes with an effective 0.45-m aperture, which are competitive—to within a factor of ∼1–10 in sensitivity for $d = 5$ models—even when compared to optical polarimetry from a 3.6-m telescope [17,56]. Since $d = 6$ models were not analyzed in [17], it would be interesting to perform similar comparisons to our $d = 6$ constraints in future work, along with comparisons to the $d = 4$ models analyzed in [109]. As such, there is a strong science case to use the maximum observed polarization for a large sample of AGN with wide optical bandpasses to constrain the anisotropic vacuum birefringent SME models, which include the three families of other SME coefficients not constrained by time delay measurements.

Future work could improve upon existing SME constraints simply by using the methods in this work to analyze optical polarimetry from large published surveys of AGN and quasars (e.g., [110,111]) in addition to the AGN and GRB afterglow sources already studied by [17,109]. In addition, state-of-the-art SME constraints could potentially be obtained by performing a new survey to significantly increase the number of high redshift sources with published optical polarimetry along independent lines of sight. The pilot program described in this work thus serves to motivate a dedicated optical AGN polarimetric survey similar to the Steward Observatory spectropolarimetric AGN monitoring program [56], the RoboPol survey of gamma-ray selected blazars [67,110,112], or the La Silla Observatory survey of optical linear polarization of QSOs [56,111], to name some relevant examples.

Such future surveys would obtain broadband optical polarimetry of each AGN source with a set of filters, optics, and detectors optimally chosen to improve upon the SME constraints obtainable using the more standard optical filters employed by previous surveys. In addition to measuring sources along lines of sight without previously published polarimetry, where possible, polarimetric measurements of previously observed sources could still lead to tighter SME constraints by either observing a larger maximum polarization than what was reported in the literature or by observing with a wider optical bandpass.

By duplicating this setup on one or more 1-meter class telescopes in each hemisphere, using the same data reduction software, such a survey could achieve the full sky coverage needed to fully constrain the more general anisotropic SME models at increasingly larger mass dimension $d \geq 4$. However, unlike previous surveys, it may only be necessary to observe a short duration time series for each AGN source, in order to maximize the number of sources with maximum polarization measurements, thereby optimizing a to-be-determined figure of merit which would quantify the improvement in constraints for specific SME models, during a given survey time period.

Since spectropolarimetry typically yields SME $d = 5$ model parameter constraints that are ∼2–3 orders of magnitude more sensitive than using a single, broadband, optical filter [17], it would also be interesting to investigate the costs and benefits of a full spectropolarimetric survey on $\gtrsim$2-m class telescopes vs a less expensive, shorter duration survey on a set of 1-m class telescopes using multiple optical filters to test $d \geq 4$ SME models. Similarly, it would be worthwhile in future work to explore the tradeoffs for constraining SME models by using multiple, nonoverlapping, narrow-band, optical filters to effectively perform low resolution spectropolarimetry vs combining two or more filters into a single, broadband filter, as demonstrated in this work.

Design feasibility studies for such a proposed survey will be analyzed in future work, with emphasis on the best path to quickly achieve the largest payoff for astrophysical tests of *CPT* and Lorentz invariance violation without the time and expense required to perform an all-sky spectropolarimetric survey.

ACKNOWLEDGMENTS

This work was originally inspired in part by conversations with Chris Stubbs. We thank Calvin Leung for sharing code to help compute transmission functions. A. S. F. acknowledges support from NSF INSPIRE Grant No. PHYS 1541160. B. G. K. acknowledges support from UCSD's Ax Center for Experimental Cosmology. We made use of the NASA/IPAC Extragalactic Database (NED), which is operated by the Jet Propulsion Laboratory, California Institute of Technology, under contract with NASA. This research also made use of the Simbad and VizieR databases, operated at CDS, Strasbourg, France. We also acknowledge extensive use of the HPOL spectropolarimetric database, http://www.sal.wisc.edu/HPOL, for instrument development and calibration. We further acknowledge the variable star observations from the AAVSO International Database contributed by observers worldwide and used in this research.

APPENDIX A: *CPT*-EVEN Q AND U

We can calculate the Stokes Q and U parameters in the presence of *CPT*-even SME coefficients of the form $\bar{k}^{(d)}_{(EB),s}$ as defined in Eq. (12). As was written in Eq. (13), the phase delay between the two normal modes is given by the equation

$$\Phi(\omega) = 2\omega^{d-3} L^{(d)} \bar{k}^{(d)}_{(EB),s}, \tag{A1}$$

where we denote the energy as ω as opposed to E in this case to distinguish it from the electric field.

The most conservative limits on SME coefficients are obtained when we assume a broadband source emitting a uniformly linearly polarized electric field along our line of sight $\hat{z}$ in the form

$$\vec{E}(\omega, t) = A e^{i\omega t} \hat{n}, \tag{A2}$$

where $\hat{n}$ makes an angle ψ_0 with respect to the detector reference angle. Then, if the slow axis of this CPT-even Lorentz violation makes an angle ψ_b with respect to the detector reference angle so that we can define the quantity

$$\Psi = \psi_0 - \psi_b, \tag{A3}$$

the signal that reaches our detector along the slow and fast axes can be written

$$E_{\text{slow}}(\omega, t) = A e^{i\omega t - i\Phi/2} \cos\Psi, \tag{A4}$$

$$E_{\text{fast}}(\omega, t) = A e^{i\omega t + i\Phi/2} \sin\Psi, \tag{A5}$$

which, relative to our detector, is the electric field

$$\begin{aligned}\vec{E}(\omega, t) = {} & A e^{i\omega t}[e^{-i\Phi/2} \cos\Psi \cos\psi_b - e^{i\Phi/2} \sin\Psi \sin\psi_b]\hat{x} \\ & + A e^{i\omega t}[e^{-i\Phi/2} \cos\Psi \sin\psi_b \\ & + e^{i\Phi/2} \sin\Psi \cos\psi_b]\hat{y}.\end{aligned} \tag{A6}$$

Next, we can define the averaging over the transmission band $T(\omega)$ as the operation

$$\langle X \rangle_\omega = \frac{\int d\omega T(\omega) X(\omega)}{\int d\omega T(\omega)}, \tag{A7}$$

so the Stokes parameters in terms of the band averaged electric field $\vec{E}(t) = \langle \vec{E}(\omega, t) \rangle_\omega$ incident on our detector are

$$I = |E_x|^2 + |E_y|^2 = |A|^2, \tag{A8}$$

$$\begin{aligned}Q &= |E_x|^2 - |E_y|^2 \\ &= I \cos 2\Psi \cos 2\psi_b - I |\langle \cos\Phi \rangle|^2 \sin 2\Psi \sin 2\psi_b,\end{aligned} \tag{A9}$$

$$\begin{aligned}U &= 2\text{Re}(E_x E_y^*) \\ &= I \cos 2\Psi \sin 2\psi_b + I |\langle \cos\Phi \rangle|^2 \sin 2\Psi \cos 2\psi_b,\end{aligned} \tag{A10}$$

$$V = 2\text{Im}(E_x E_y^*) = I |\langle \sin\Phi \rangle|^2 \sin 2\Psi. \tag{A11}$$

Therefore, the normalized Stokes parameters $q = Q/I$, $u = U/I$ and total linear polarization fraction p are

$$q = \cos 2\Psi \cos 2\psi_b - |\langle \cos\Phi \rangle|^2 \sin 2\Psi \sin 2\psi_b, \tag{A12}$$

$$u = \cos 2\Psi \sin 2\psi_b + |\langle \cos\Phi \rangle|^2 \sin 2\Psi \cos 2\psi_b, \tag{A13}$$

$$p = \sqrt{\cos^2 2\Psi + \langle \cos\Phi \rangle^2 \sin^2 2\Psi}. \tag{A14}$$

Due to the many unknowns in Eq. (A14), it is impractical to use time delays between each q and u time series, for example, to constrain SME vacuum birefringent parameters. Circular polarization measurements could potentially break certain degeneracies, but the maximum observed polarization approach will, in general, yield more sensitive SME constraints than any approaches using optical time delays.

APPENDIX B: DATA PLOTS AND TABLES

All data in this paper were observed with APPOL from December 2017 to January 2018. Samples of the observed data for BL Lacertae and S5 B0716 + 714 are shown in Tables V–VIII, and the full machine-readable data are available at [63]. Polarimetry is plotted in Figs. 9 and 10 for BL Lacertae and in Figs. 12 and 13 for S5 B0716 + 714, with photometry in Figs. 11 and 14, respectively.

TABLE V. Three nights of data for BL Lacertae were observed using APPOL on December 13, 14, and 17, 2017. For each modified Julian date (MJD), we show our observed polarimetric and photometric data for both the *Lum* and I_c bands, denoted by L and I subscripts, respectively. Columns include the observed polarization p (in %), the polarization angle ψ (in degrees), the intensity normalized Stokes parameters q and u (note that both can be negative, even when expressed as percentages), and the observed magnitude m. (A portion of this table is shown for guidance. This table is available in its entirety in machine-readable form.)

MJD (days)	p_L (%)	p_I (%)	ψ_L (deg)	ψ_I (deg)	q_L (%)	q_I (%)	u_L (%)	u_I (%)	m_L (mag)	m_I (mag)
58101.072	10.3 ± 0.6	9.5 ± 0.4	59.0 ± 2.0	59.0 ± 1.0	-4.9 ± 0.6	-4.4 ± 0.4	9.0 ± 0.5	8.4 ± 0.4	13.69 ± 0.03	12.93 ± 0.04
58101.079	9.0 ± 0.4	7.7 ± 0.3	63.0 ± 1.0	58.0 ± 1.0	-5.2 ± 0.4	-3.4 ± 0.3	7.3 ± 0.4	6.9 ± 0.3	13.82 ± 0.03	12.96 ± 0.04
58101.085	8.2 ± 0.4	7.9 ± 0.3	60.0 ± 1.0	59.0 ± 1.0	-4.1 ± 0.4	-3.7 ± 0.3	7.1 ± 0.4	7.0 ± 0.3	13.74 ± 0.03	12.95 ± 0.04

TABLE VI. Same as Table V, but with all data for S5 B0716 + 714, which we observed using APPOL over five nights—December 11–14 2017 and January 1, 2018. (A portion of this table is shown for guidance. This table is available in its entirety in machine-readable form.)

MJD (days)	p_L (%)	p_I (%)	ψ_L (deg)	ψ_I (deg)	q_L (%)	q_I (%)	u_L (%)	u_I (%)	m_L (mag)	m_I (mag)
58099.300	8.8 ± 0.7	8.3 ± 0.5	88.0 ± 2.0	92.0 ± 2.0	-8.8 ± 0.7	-8.3 ± 0.5	0.8 ± 0.7	-0.7 ± 0.5	14.93 ± 0.04	14.39 ± 0.05
58099.306	6.9 ± 0.7	5.3 ± 0.5	81.0 ± 3.0	88.0 ± 3.0	-6.6 ± 0.7	-5.3 ± 0.5	2.1 ± 0.8	0.3 ± 0.6	15.00 ± 0.04	14.39 ± 0.05
58099.319	8.5 ± 0.7	7.6 ± 0.5	84.0 ± 2.0	88.0 ± 2.0	-8.3 ± 0.7	-7.6 ± 0.5	1.9 ± 0.7	0.6 ± 0.5	14.93 ± 0.04	14.32 ± 0.05

TABLE VII. Same as Table V for BL Lacertae, but for the combined $Lum + I_c$ band. (A portion of this table is shown for guidance. This table is available in its entirety in machine-readable form.)

MJD (days)	p_{L+I} (%)	ψ_{L+I} (deg)	q_{L+I} (%)	u_{L+I} (%)
58101.072	9.9 ± 0.4	59.0 ± 1.0	-4.7 ± 0.4	8.8 ± 0.4
58101.079	8.4 ± 0.3	61.0 ± 1.0	-4.5 ± 0.3	7.1 ± 0.3
58101.085	8.1 ± 0.3	59.5 ± 0.9	-3.9 ± 0.3	7.1 ± 0.3

TABLE VIII. Same as Table VI for S5 B0716 + 714, but for the combined $Lum + I_c$ band. (A portion of this table is shown for guidance. This table is available in its entirety in machine-readable form.)

MJD (days)	p_{L+I} (%)	ψ_{L+I} (deg)	q_{L+I} (%)	u_{L+I} (%)
58099.300	8.6 ± 0.4	89.0 ± 1.0	-8.6 ± 0.4	0.2 ± 0.4
58099.306	6.2 ± 0.5	84.0 ± 2.0	-6.1 ± 0.5	1.3 ± 0.5
58099.319	8.1 ± 0.4	85.0 ± 2.0	-8.0 ± 0.4	1.3 ± 0.4

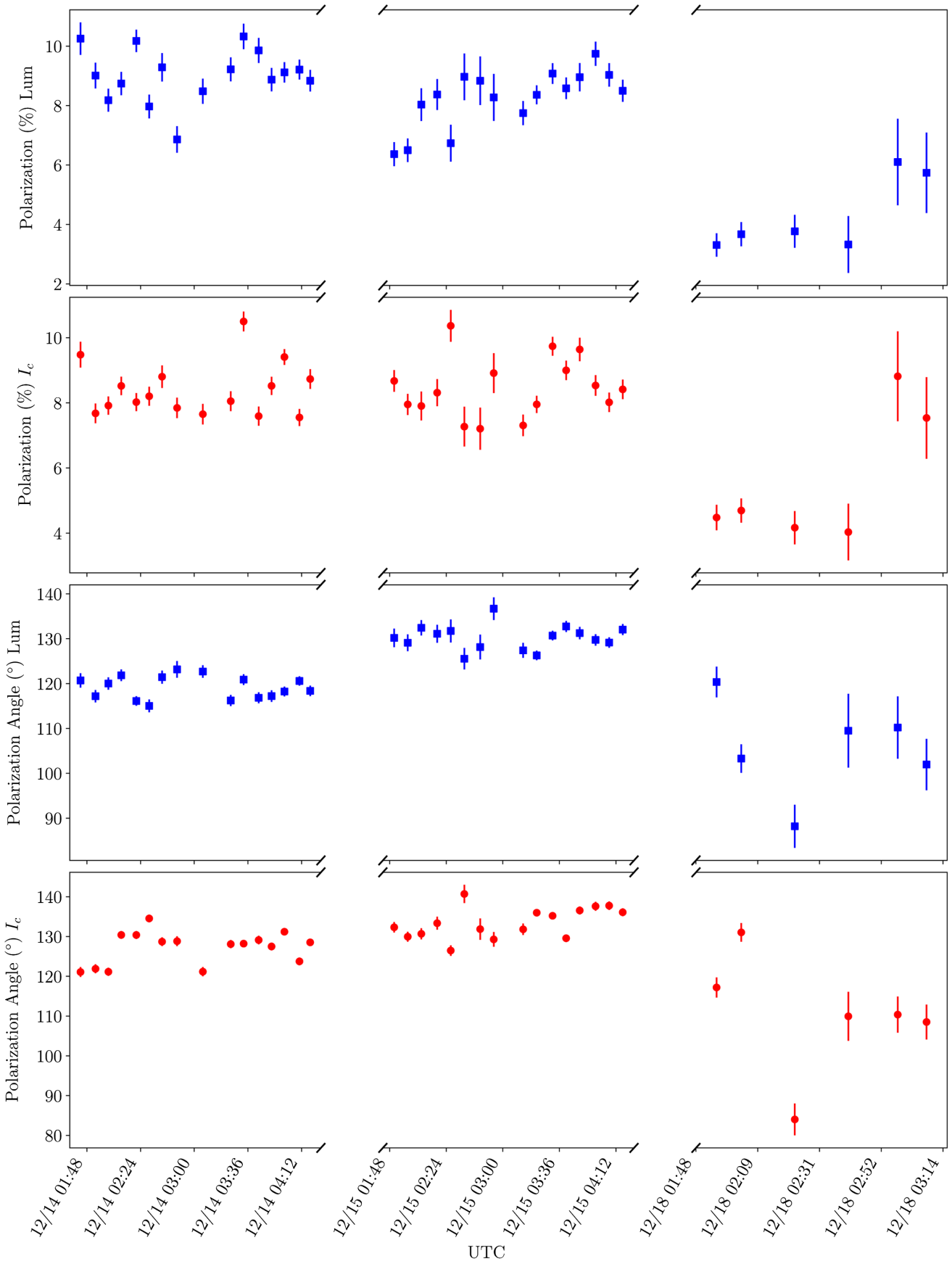

FIG. 9. Polarization p (in %) and polarization angle ψ (in degrees) for BL Lacertae in the *Lum* and I_c bands. Intensity normalized Stokes parameters $q \equiv Q/I$ and $u \equiv U/I$ for both bands are available in the full machine-readable tables [63].

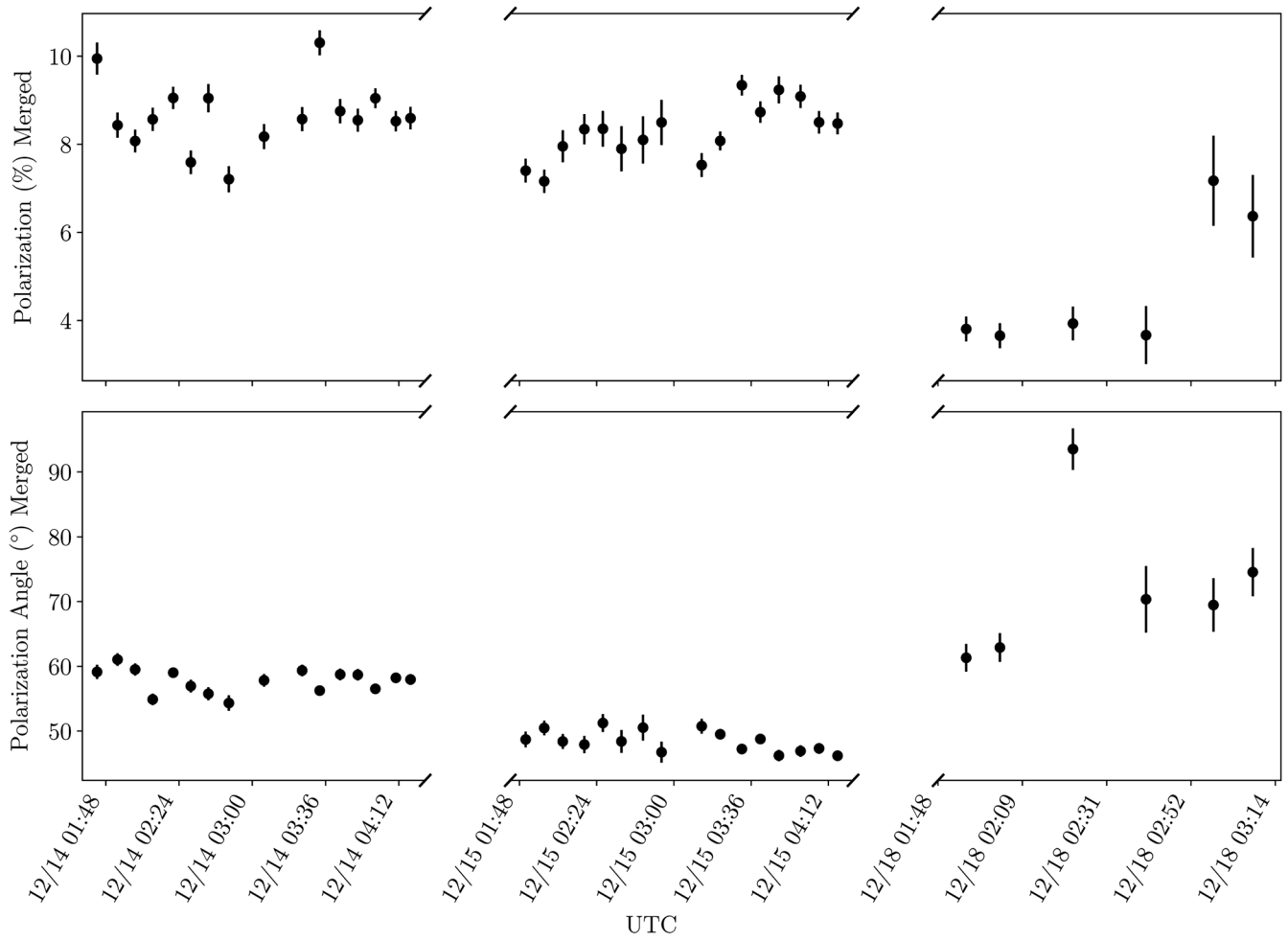

FIG. 10. BL Lacertae light curves for polarization p (in %) and polarization angle ψ (in degrees). Intensity normalized Stokes parameters $q \equiv Q/I$ and $u \equiv U/I$ for the *combined* $Lum + I_c$ band are available in the full machine-readable tables [63].

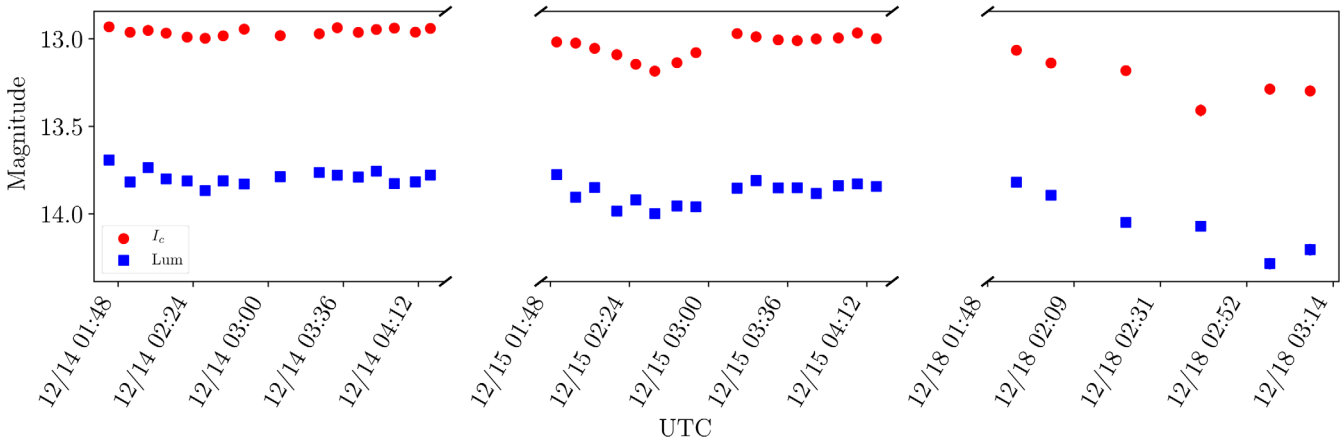

FIG. 11. I_c and *Lum*-band photometry for BL Lacertae.

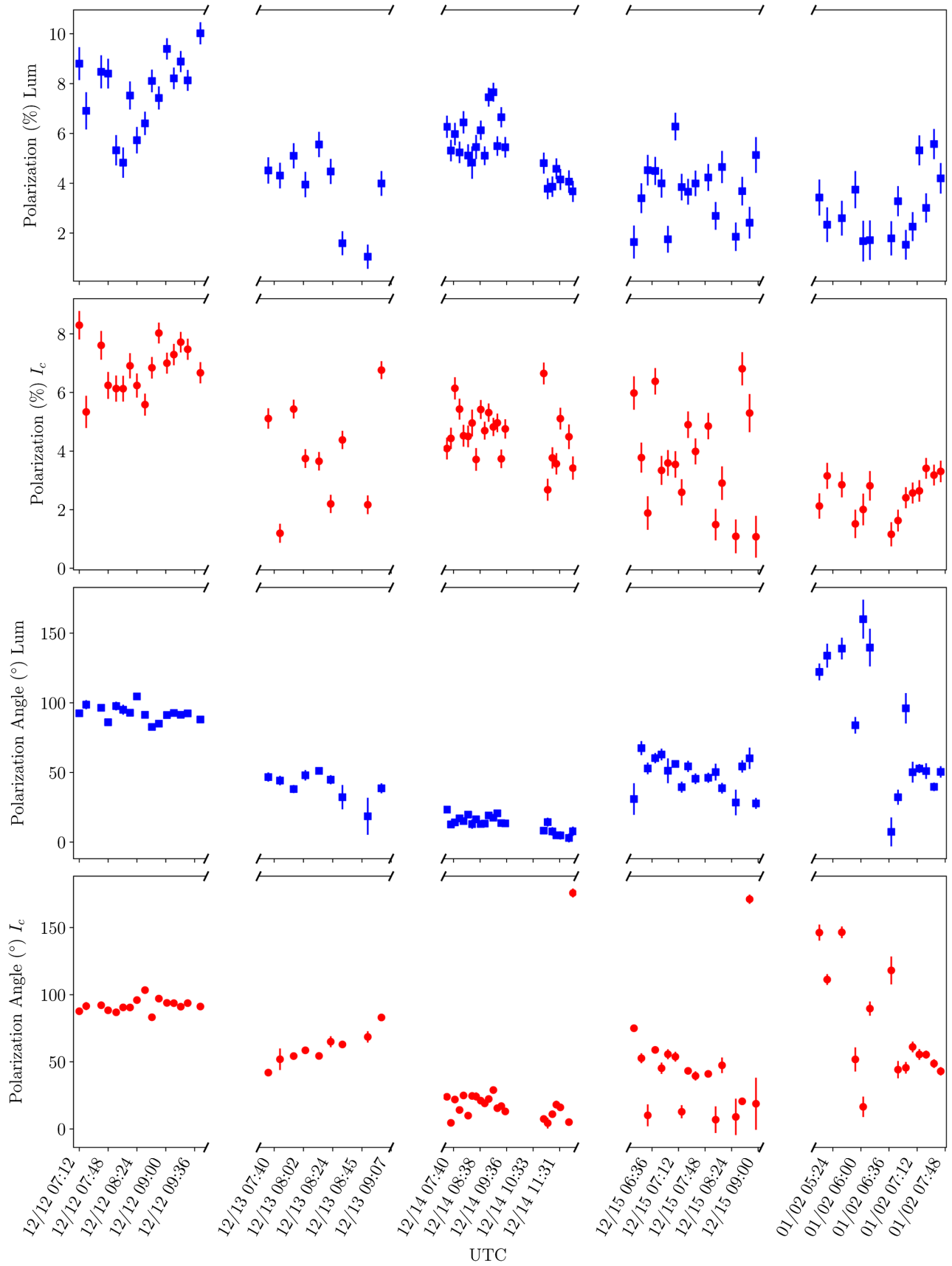

FIG. 12. Polarization p (in %) and polarization angle ψ (in degrees) for S5 B0716 + 714 in the *Lum* and I_c bands. Intensity normalized Stokes parameters $q \equiv Q/I$ and $u \equiv U/I$ for both bands are available in the full machine-readable tables [63].

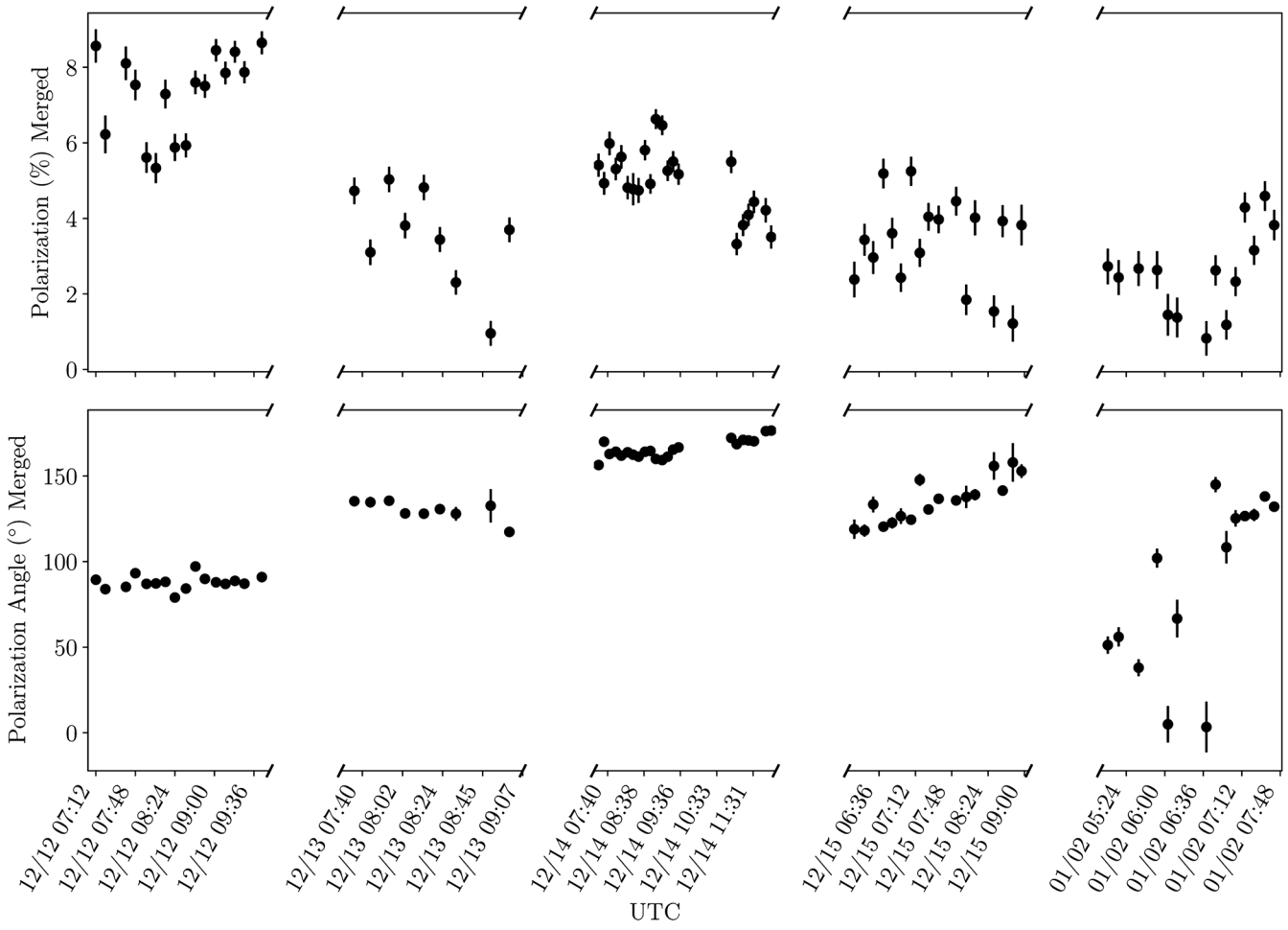

FIG. 13. S5 B0716 + 714 light curves for polarization p (in %) and polarization angle ψ (in degrees). Intensity normalized Stokes parameters $q \equiv Q/I$ and $u \equiv U/I$ in the *Merged Lum* + I_c band are available in the full machine-readable tables [63].

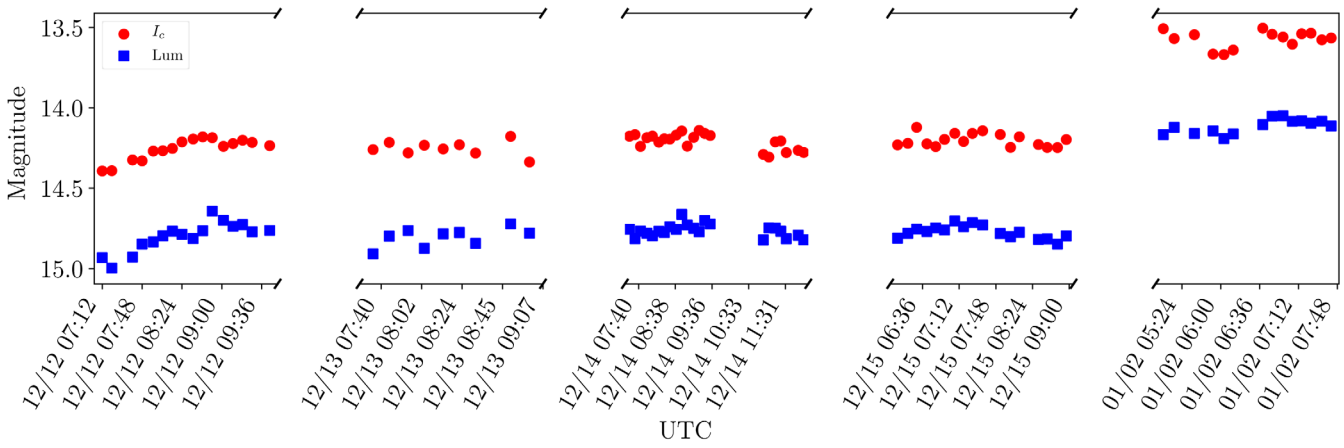

FIG. 14. I_c and *Lum*-band photometry for S5 B0716 + 714.

[1] V. A. Kostelecký and N. Russell, Data tables for Lorentz and *CPT* violation, Rev. Mod. Phys. **83**, 11 (2011).

[2] R. C. Myers and M. Pospelov, Ultraviolet Modifications of Dispersion Relations in Effective Field Theory, Phys. Rev. Lett. **90**, 211601 (2003).

[3] G. Amelino-Camelia, D. Guetta, and T. Piran, ICECUBE neutrinos and Lorentz invariance violation, Astrophys. J. **806**, 269 (2015).

[4] U. Jacob and T. Piran, Neutrinos from gamma-ray bursts as a tool to explore quantum-gravity-induced Lorentz violation, Nat. Phys. **3**, 87 (2007).

[5] U. Jacob and T. Piran, Lorentz-violation-induced arrival delays of cosmological particles, J. Cosmol. Astropart. Phys. 1 (2008) 031.

[6] S. Chakraborty, A. Mirizzi, and G. Sigl, Testing Lorentz invariance with neutrino bursts from supernova neutronization, Phys. Rev. D **87**, 017302 (2013).

[7] F. W. Stecker and S. T. Scully, Propagation of superluminal PeV IceCube neutrinos: A high energy spectral cutoff or new constraints on Lorentz invariance violation, Phys. Rev. D **90**, 043012 (2014).

[8] S. T. Scully and F. W. Stecker, Lorentz invariance violation and the observed spectrum of ultrahigh energy cosmic rays, Astropart. Phys. **31**, 220 (2009).

[9] F. W. Stecker, Gamma-ray and cosmic-ray tests of Lorentz invariance violation and quantum gravity models and their implications, AIP Conf. Proc. **1223**, 192 (2010).

[10] W. Bietenholz, Cosmic rays and the search for a Lorentz invariance violation, Phys. Rep. **505**, 145 (2011).

[11] R. Cowsik, T. Madziwa-Nussinov, S. Nussinov, and U. Sarkar, Testing violations of Lorentz invariance with cosmic rays, Phys. Rev. D **86**, 045024 (2012).

[12] R. G. Lang and V. de Souza, Astroparticle physics tests of Lorentz invariance violation, J. Phys. Conf. Ser. **866**, 012008 (2017).

[13] V. A. Kostelecký and M. Mewes, Astrophysical tests of Lorentz and *CPT* violation with photons, Astrophys. J. Lett. **689**, L1 (2008).

[14] C. Pfeifer, Redshift and lateshift from homogeneous and isotropic modified dispersion relations, Phys. Lett. B **780**, 246 (2018).

[15] S. M. Carroll, G. B. Field, and R. Jackiw, Limits on a Lorentz- and parity-violating modification of electrodynamics, Phys. Rev. D **41**, 1231 (1990).

[16] V. A. Kostelecký and M. Mewes, Electrodynamics with Lorentz-violating operators of arbitrary dimension, Phys. Rev. D **80**, 015020 (2009).

[17] F. Kislat and H. Krawczynski, Planck-scale constraints on anisotropic Lorentz and CPT invariance violations from optical polarization measurements, Phys. Rev. D **95**, 083013 (2017).

[18] G. Amelino-Camelia, *Doubly-Special Relativity: Facts, Myths and Some Key Open Issues* (World Scientific Publishing, Singapore, 2010), pp. 123–170.

[19] L. Smolin, Classical paradoxes of locality and their possible quantum resolutions in deformed special relativity, Gen. Relativ. Gravit. **43**, 3671 (2011).

[20] E. Komatsu, J. Dunkley, M. R. Nolta, C. L. Bennett, B. Gold, G. Hinshaw, N. Jarosik, D. Larson, M. Limon, L. Page *et al.*, Five-year Wilkinson microwave anisotropy probe observations: Cosmological interpretation, Astrophys. J. Suppl. Ser. **180**, 330 (2009).

[21] G. Gubitosi, L. Pagano, G. Amelino-Camelia, A. Melchiorri, and A. Cooray, A constraint on Planck-scale modifications to electrodynamics with CMB polarization data, J. Cosmol. Astropart. Phys. 08 (2009) 021.

[22] T. Kahniashvili, R. Durrer, and Y. Maravin, Testing Lorentz invariance violation with Wilkinson microwave anisotropy probe five year data, Phys. Rev. D **78**, 123009 (2008).

[23] J. P. Kaufman, B. G. Keating, and B. R. Johnson, Precision tests of parity violation over cosmological distances, Mon. Not. R. Astron. Soc. **455**, 1981 (2016).

[24] D. Leon, J. Kaufman, B. Keating, and M. Mewes, The cosmic microwave background and pseudo-Nambu-Goldstone bosons: Searching for Lorentz violations in the cosmos, Mod. Phys. Lett. A **32**, 1730002 (2017).

[25] J. Kaufman, D. Leon, and B. Keating, Using the Crab Nebula as a high precision calibrator for cosmic microwave background polarimeters, Int. J. Mod. Phys. D **25**, 1640008 (2016).

[26] J. P. Kaufman, N. J. Miller, M. Shimon, D. Barkats, C. Bischoff, I. Buder, B. G. Keating, J. M. Kovac, P. A. R. Ade, R. Aikin *et al.*, Self-calibration of BICEP1 three-year data and constraints on astrophysical polarization rotation, Phys. Rev. D **89**, 062006 (2014).

[27] G. Amelino-Camelia, J. Ellis, N. E. Mavromatos, D. V. Nanopoulos, and S. Sarkar, Tests of quantum gravity from observations of γ-ray bursts, Nature (London) **393**, 763 (1998).

[28] S. E. Boggs, C. B. Wunderer, K. Hurley, and W. Coburn, Testing Lorentz invariance with GRB 021206, Astrophys. J. Lett. **611**, L77 (2004).

[29] J. Ellis, N. E. Mavromatos, D. V. Nanopoulos, A. S. Sakharov, and E. K. G. Sarkisyan, Robust limits on Lorentz violation from gamma-ray bursts, Astropart. Phys. **25**, 402 (2006).

[30] M. Rodríguez Martínez and T. Piran, Constraining Lorentz violations with gamma ray bursts, J. Cosmol. Astropart. Phys. 04 (2006) 006.

[31] T. Kahniashvili, G. Gogoberidze, and B. Ratra, Gamma ray burst constraints on ultraviolet Lorentz invariance violation, Phys. Lett. B **643**, 81 (2006).

[32] M. Biesiada and A. Piórkowska, Gamma-ray burst neutrinos, Lorenz invariance violation and the influence of background cosmology, J. Cosmol. Astropart. Phys. 05 (2007) 011.

[33] Z. Xiao and B.-Q. Ma, Constraints on Lorentz invariance violation from gamma-ray burst GRB090510, Phys. Rev. D **80**, 116005 (2009).

[34] P. Laurent, D. Götz, P. Binétruy, S. Covino, and A. Fernandez-Soto, Constraints on Lorentz invariance violation using integral/IBIS observations of GRB041219A, Phys. Rev. D **83**, 121301 (2011).

[35] F. W. Stecker, A new limit on Planck scale Lorentz violation from γ-ray burst polarization, Astropart. Phys. **35**, 95 (2011).

[36] K. Toma, S. Mukohyama, D. Yonetoku, T. Murakami, S. Gunji, T. Mihara, Y. Morihara, T. Sakashita, T. Takahashi, Y. Wakashima *et al.*, Strict Limit on CPT Violation from

Polarization of γ-Ray Bursts, Phys. Rev. Lett. **109**, 241104 (2012).
[37] V. A. Kostelecký and M. Mewes, Constraints on Relativity Violations from Gamma-Ray Bursts, Phys. Rev. Lett. **110**, 201601 (2013).
[38] V. Vasileiou, A. Jacholkowska, F. Piron, J. Bolmont, C. Couturier, J. Granot, F. W. Stecker, J. Cohen-Tanugi, and F. Longo, Constraints on Lorentz invariance violation from Fermi-Large Area Telescope observations of gamma-ray bursts, Phys. Rev. D **87**, 122001 (2013).
[39] Y. Pan, Y. Gong, S. Cao, H. Gao, and Z.-H. Zhu, Constraints on the Lorentz invariance violation with gamma-ray bursts via a Markov Chain Monte Carlo approach, Astrophys. J. **808**, 78 (2015).
[40] S. Zhang and B.-Q. Ma, Lorentz violation from gamma-ray bursts, Astropart. Phys. **61**, 108 (2015).
[41] Z. Chang, X. Li, H.-N. Lin, Y. Sang, P. Wang, and S. Wang, Constraining Lorentz invariance violation from the continuous spectra of short gamma-ray bursts, Chin. Phys. C **40**, 045102 (2016).
[42] H.-N. Lin, X. Li, and Z. Chang, Gamma-ray burst polarization reduction induced by the Lorentz invariance violation, Mon. Not. R. Astron. Soc. **463**, 375 (2016).
[43] J.-J. Wei, B.-B. Zhang, L. Shao, X.-F. Wu, and P. Mészáros, A new test of Lorentz invariance violation: The spectral lag transition of GRB 160625B, Astrophys. J. Lett. **834**, L13 (2017).
[44] S. D. Biller, A. C. Breslin, J. Buckley, M. Catanese, M. Carson, D. A. Carter-Lewis, M. F. Cawley, D. J. Fegan, J. P. Finley, J. A. Gaidos *et al.*, Limits to Quantum Gravity Effects on Energy Dependence of the Speed of Light from Observations of TeV Flares in Active Galaxies, Phys. Rev. Lett. **83**, 2108 (1999).
[45] J. Albert, E. Aliu, H. Anderhub, L. A. Antonelli, P. Antoranz, M. Backes, C. Baixeras, J. A. Barrio, H. Bartko *et al.* (MAGIC Collaboration), Probing quantum gravity using photons from a flare of the active galactic nucleus Markarian 501 observed by the MAGIC telescope, Phys. Lett. B **668**, 253 (2008).
[46] F. Aharonian, A. G. Akhperjanian, U. Barres de Almeida, A. R. Bazer-Bachi, Y. Becherini, B. Behera, M. Beilicke, W. Benbow, K. Bernlöhr, C. Boisson *et al.*, Limits on an Energy Dependence of the Speed of Light from a Flare of the Active Galaxy PKS 2155-304, Phys. Rev. Lett. **101**, 170402 (2008).
[47] L. Shao, Z. Xiao, and B.-Q. Ma, Lorentz violation from cosmological objects with very high energy photon emissions, Astropart. Phys. **33**, 312 (2010).
[48] M. Fairbairn, A. Nilsson, J. Ellis, J. Hinton, and R. White, The CTA sensitivity to Lorentz-violating effects on the gamma-ray horizon, J. Cosmol. Astropart. Phys. 06 (2014) 005.
[49] F. Tavecchio and G. Bonnoli, On the detectability of Lorentz invariance violation through anomalies in the multi-TeV γ-ray spectra of blazars, Astron. Astrophys. **585**, A25 (2016).
[50] M. Biesiada and A. Piórkowska, Gravitational lensing time delays as a tool for testing Lorentz-invariance violation, Mon. Not. R. Astron. Soc. **396**, 946 (2009).
[51] L. Shao, Tests of Local Lorentz Invariance Violation of Gravity in the Standard Model Extension with Pulsars, Phys. Rev. Lett. **112**, 111103 (2014).
[52] R. C. Vermeulen, P. M. Ogle, H. D. Tran, I. W. A. Browne, M. H. Cohen, A. C. S. Readhead, G. B. Taylor, and R. W. Goodrich, When is BL Lac not a BL Lac?, Astrophys. J. Lett. **452**, L5 (1995).
[53] K. Nilsson, T. Pursimo, A. Sillanpää, L. O. Takalo, and E. Lindfors, Detection of the host galaxy of S5 0716 + 714, Astron. Astrophys. **487**, L29 (2008).
[54] C. W. Danforth, K. Nalewajko, K. France, and B. A. Keeney, A fast flare and direct redshift constraint in far-ultraviolet spectra of the blazar S5 0716 + 714, Astrophys. J. **764**, 57 (2013).
[55] G. D. Schmidt, H. S. Stockman, and P. S. Smith, Discovery of a sub-megagauss magnetic white dwarf through spectropolarimetry, Astrophys. J. Lett. **398**, L57 (1992).
[56] D. Sluse, D. Hutsemékers, H. Lamy, R. Cabanac, and H. Quintana, New optical polarization measurements of quasi-stellar objects. The data, Astron. Astrophys. **433**, 757 (2005).
[57] P. S. Smith, E. Montiel, S. Rightley, J. Turner, G. D. Schmidt, and B. T. Jannuzi, Coordinated Fermi/optical monitoring of blazars and the great 2009 September gamma-ray flare of 3C 454.3, arXiv:0912.3621.
[58] V. Piirola, A. Berdyugin, and S. Berdyugina, DIPOL-2: A double image high precision polarimeter, in *Ground-Based and Airborne Instrumentation for Astronomy V*, edited by S. K. Ramsay, I. S. McLean, and H. Takami, Proceedings of SPIE Vol. 9147 (2014), p. 91478I.
[59] A. G. Riess, L. M. Macri, S. L. Hoffmann, D. Scolnic, S. Casertano, A. V. Filippenko, B. E. Tucker, M. J. Reid, D. O. Jones, J. M. Silverman *et al.*, A 2.4% determination of the local value of the Hubble constant, Astrophys. J. **826**, 56 (2016).
[60] P. A. R. Ade, N. Aghanim, M. Arnaud, M. Ashdown, J. Aumont, C. Baccigalupi, A. J. Banday, R. B. Barreiro, J. G. Bartlett *et al.* (Planck Collaboration), Planck 2015 results. XIII. Cosmological parameters, Astron. Astrophys. **594**, A13 (2016).
[61] R. A. Edelson and J. H. Krolik, The discrete correlation function—A new method for analyzing unevenly sampled variability data, Astrophys. J. **333**, 646 (1988).
[62] D. R. S. Robertson, L. C. Gallo, A. Zoghbi, and A. C. Fabian, Searching for correlations in simultaneous X-ray and UV emission in the narrow-line Seyfert 1 galaxy 1H 0707-495, Mon. Not. R. Astron. Soc. **453**, 3455 (2015).
[63] See Supplemental Material at http://link.aps.org/supplemental/10.1103/PhysRevD.99.035045 for machine-readable data tables corresponding to full versions of Tables V–VIII of this paper.
[64] J. Tinbergen, Astronomical Polarimetry (Cambridge University Press, Cambridge, England, 2005).
[65] D. S. Berry, T. M. Gledhill, J. S. Greaves, and T. Jenness, POLPACK—An imaging polarimetry reduction package, in *Astronomical Polarimetry: Current Status and Future Directions*, edited by A. Adamson, C. Aspin, C. Davis, and T. Fujiyoshi, Astronomical Society of the Pacific Conference Series Vol. 343 (2005), p. 71, http://aspbooks.org/custom/publications/paper/343-0071.html.

[66] D. S. Berry and T. M. Gledhill, POLPACK: Imaging polarimetry reduction package, Astrophys. Source Code Libr. (2014), http://ascl.net/1405.014.

[67] O. G. King, D. Blinov, A. N. Ramaprakash, I. Myserlis, E. Angelakis, M. Baloković, R. Feiler, L. Fuhrmann, T. Hovatta, P. Khodade *et al.*, The RoboPol pipeline and control system, Mon. Not. R. Astron. Soc. **442**, 1706 (2014).

[68] G. Panopoulou, K. Tassis, D. Blinov, V. Pavlidou, O. G. King, E. Paleologou, A. Ramaprakash, E. Angelakis, M. Baloković, H. K. Das *et al.*, Optical polarization map of the Polaris Flare with RoboPol, Mon. Not. R. Astron. Soc. **452**, 715 (2015).

[69] R. Skalidis, G. V. Panopoulou, K. Tassis, V. Pavlidou, D. Blinov, I. Komis, and I. Liodakis, Local measurements of the mean interstellar polarization at high Galactic latitudes, Astron. Astrophys. **616**, A52 (2018).

[70] G. M. Cole, Developing a polarimeter to support the epsilon Aurigae Campaign, in the Society for Astronomical Sciences 29th Annual Symposium on Telescope Science, Big Bear Lake, CA, 2010 (Society for Astronomical Sciences Annual Symposium, 2010), http://articles.adsabs.harvard.edu/cgi-bin/nph-iarticle_query?2010SASS...29...37C&data_type=PDF_HIGH&whole_paper=YES&type=PRINTER&filetype=.pdf.

[71] G. M. Cole, A pellicle autoguider for the DSS-7 spectrograph, in *the Society for Astronomical Sciences 26th Annual Symposium on Telescope Science, Big Bear, CA* (2007), http://articles.adsabs.harvard.edu/cgi-bin/nph-iarticle_query?2007SASS...26..153C&data_type=PDF_HIGH&whole_paper=YES&type=PRINTER&filetype=.pdf.

[72] G. M. Cole, Automating a telescope for spectroscopy, in *the Society for Astronomical Sciences 27th Annual Symposium on Telescope Science, Big Bear Lake, CA* (2008), http://articles.adsabs.harvard.edu/cgi-bin/nph-iarticle_query?2008SASS...27..103C&data_type=PDF_HIGH&whole_paper=YES&type=PRINTER&filetype=.pdf.

[73] G. M. Cole, A new instrument selector for small telescopes, Am. Astron. Soc. Meet. Abstr. **214**, 672 (2009), http://adsabs.harvard.edu/abs/2009AAS...21440908C.

[74] G. Cole, A spectropolarimeter based on the SBIG spectrometer, in *IAPPP Western Wing (USA) 20th Annual Astronomical Photometry and Ccd Imaging Symposium, Big Bear Lake, California* (2001), http://articles.adsabs.harvard.edu/cgi-bin/nph-iarticle_query?2001IAPPP..84...13C&data_type=PDF_HIGH&whole_paper=YES&type=PRINTER&filetype=.pdf.

[75] G. M. Cole, Small telescope spectropolarimetry: Instruments and observations, in *the Society for Astronomical Sciences 35th Annual Symposium on Telescope Science* (2016), http://articles.adsabs.harvard.edu/cgi-bin/nph-iarticle_query?2016SASS...35...37C&data_type=PDF_HIGH&whole_paper=YES&type=PRINTER&filetype=.pdf.

[76] G. M. Cole and R. E. Stencel, Polarimetry of Epsilon Aurigae from mid eclipse to third contact, in *the Society for Astronomical Sciences 30th Annual Symposium on Telescope Science, Big Bear Lake, CA* (2011), http://articles.adsabs.harvard.edu/cgi-bin/nph-iarticle_query?2011SASS...30..103C&data_type=PDF_HIGH&whole_paper=YES&type=PRINTER&filetype=.pdf.

[77] G. M. Cole, Polarimetry of Epsilon Aurigae, from November 2009 to January 2012, J. Am. Assoc. Var. Star Obs. **40**, 787 (2012).

[78] G. M. Cole, Long term broadband polarimetry of Epsilon Aurigae and field stars, in *Giants of Eclipse* (2013), Vol. 45, http://adsabs.harvard.edu/abs/2013giec.conf20203C.

[79] T. M. Wolfe, R. Stencel, and G. Cole, *Commissioning Results of a New Polarimeter: Denver University Small Telescope Polarimeter (DUSTPol)*, Polarimetry: IAU Symposium, Vol. 305, edited by K. N. Nagendra, S. Bagnulo, R. Centeno, and M. Jesús Martínez González (2015), pp. 200–206.

[80] A. S. Friedman and G. M. Cole *et al.*, The array photo polarimeter (to be published).

[81] M. Uemura, K. S. Kawabata, M. Sasada, Y. Ikejiri, K. Sakimoto, R. Itoh, M. Yamanaka, T. Ohsugi, S. Sato, and M. Kino, Bayesian approach to find a long-term trend in erratic polarization variations observed in blazars, Publ. Astron. Soc. Jpn. **62**, 69 (2010).

[82] R. Falomo, E. Pian, and A. Treves, An optical view of BL Lacertae objects, Astron. Astrophys. Rev. **22**, 73 (2014).

[83] T. Hovatta, E. Lindfors, D. Blinov, V. Pavlidou, K. Nilsson, S. Kiehlmann, E. Angelakis, V. Fallah Ramazani, I. Liodakis, I. Myserlis *et al.*, Optical polarization of high-energy BL Lacertae objects, Astron. Astrophys. **596**, A78 (2016).

[84] M. Kokubo, Constraints on the optical polarization source in the luminous non-blazar quasar 3C 323.1 (PG $1545+210$) from the photometric and polarimetric variability, Mon. Not. R. Astron. Soc. **467**, 3723 (2017).

[85] M. I. Carnerero, C. M. Raiteri, M. Villata, J. A. Acosta-Pulido, V. M. Larionov, P. S. Smith, F. D'Ammando, I. Agudo, M. J. Arévalo, R. Bachev *et al.*, Dissecting the long-term emission behaviour of the BL Lac object Mrk 421, Mon. Not. R. Astron. Soc. **472**, 3789 (2017).

[86] R. L. Moore, J. R. P. Angel, R. Duerr, M. J. Lebofsky, W. Z. Wisniewski, G. H. Rieke, D. J. Axon, J. Bailey, J. M. Hough, and J. T. McGraw, The noise of BL Lacertae, Astrophys. J. **260**, 415 (1982).

[87] Y. Ikejiri, M. Uemura, M. Sasada, R. Ito, M. Yamanaka, K. Sakimoto, A. Arai, Y. Fukazawa, T. Ohsugi, K. S. Kawabata *et al.*, Photopolarimetric monitoring of blazars in the optical and near-infrared bands with the kanata telescope. I. Correlations between flux, color, and polarization, Publ. Astron. Soc. Jpn. **63**, 639 (2011).

[88] Y.-H. Zhang, F.-Y. Bian, J.-Z. Li, and R.-C. Shang, Optical observations of BL Lacertae in 2004-2005, Mon. Not. R. Astron. Soc. **432**, 1189 (2013).

[89] Y. H. Zhang, L. Xu, and J. C. Li, Search for hard lags with intra-night optical observations of BL Lacertae, Astron. Nachr. **337**, 286 (2016).

[90] C. D. Impey, V. Bychkov, S. Tapia, Y. Gnedin, and S. Pustilnik, Rapid polarization variability in the BL Lacertae object S5 $0716+714$, Astron. J. **119**, 1542 (2000).

[91] R. Nesci, E. Massaro, and F. Montagni, Intraday optical variability of S5 $0716+714$, Pub. Astron. Soc. Aust. **19**, 143 (2002).

[92] M. Sasada, M. Uemura, A. Arai, Y. Fukazawa, K. S. Kawabata, T. Ohsugi, T. Yamashita, M. Isogai, S. Sato,

and M. Kino, Detection of polarimetric variations associated with the shortest time-scale variability in S5 0716 + 714, Publ. Astron. Soc. Jpn. **60**, L37 (2008).

[93] V. M. Larionov, S. G. Jorstad, A. P. Marscher, D. A. Morozova, D. A. Blinov, V. A. Hagen-Thorn, T. S. Konstantinova, E. N. Kopatskaya, L. V. Larionova, E. G. Larionova *et al.*, The outburst of the blazar S5 0716 + 71 in 2011 October: Shock in a helical jet, Astrophys. J. **768**, 40 (2013).

[94] S. Chandra, H. Zhang, P. Kushwaha, K. P. Singh, M. Bottcher, N. Kaur, and K. S. Baliyan, Multi-wavelength study of flaring activity in BL lac object S5 0716 + 714 during the 2015 outburst, Astrophys. J. **809**, 130 (2015).

[95] G. Bhatta, A. Goyal, M. Ostrowski, Ł. Stawarz, H. Akitaya, A. A. Arkharov, R. Bachev, E. Benítez, G. A. Borman, D. Carosati *et al.*, Discovery of a highly polarized optical microflare in blazar S5 0716 + 714 during the 2014 WEBT campaign, Astrophys. J. Lett. **809**, L27 (2015).

[96] G. Bhatta, Ł. Stawarz, M. Ostrowski, A. Markowitz, H. Akitaya, A. A. Arkharov, R. Bachev, E. Benítez, G. A. Borman, D. Carosati *et al.*, Multifrequency photo-polarimetric WEBT observation campaign on the blazar S5 0716 + 714: Source microvariability and search for characteristic timescales, Astrophys. J. **831**, 92 (2016).

[97] V. T. Doroshenko and N. N. Kiselev, Polarization and brightness of the blazar S5 0716 + 714 in 1991-2004, Astron. Lett. **43**, 365 (2017).

[98] Y.-H. Yuan, J.-h. Fan, J. Tao, B.-C. Qian, D. Costantin, H.-B. Xiao, Z.-Y. Pei, and C. Lin, Optical monitoring of BL Lac object S5 0716 + 714 and FSRQ 3C 273 from 2000 to 2014, Astron. Astrophys. **605**, A43 (2017).

[99] J. H. Hough, Polarimetry techniques at optical and infrared wavelengths, in *Astronomical Polarimetry: Current Status and Future Directions*, edited by A. Adamson, C. Aspin, C. Davis, and T. Fujiyoshi, Astronomical Society of the Pacific Conference Series Vol. 343 (2005), p. 3, http://aspbooks.org/custom/publications/paper/343-0003.html.

[100] J. Hough, Polarimetry: A powerful diagnostic tool in astronomy, Astron. Geophys. **47**, 3.31 (2006).

[101] J. H. Hough, New opportunities for astronomical polarimetry, J. Quant. Spectrosc. Radiat. Transfer **106**, 122 (2007).

[102] J. Hough, High sensitivity polarimetry: Techniques and applications, edited by M. Mishchenko, Y. Yatskiv, V. Rosenbush, and G. Videen, Polarimetric Detection, Characterization and Remote Sensing. NATO Science for Peace and Security Series C: Environmental Security (Springer, Dordrecht, 2011), pp. 177–204.

[103] S. Bagnulo, M. Landolfi, J. D. Landstreet, E. Landi Degl'Innocenti, L. Fossati, and M. Sterzik, Stellar spectropolarimetry with retarder waveplate and beam splitter devices, Publ. Astron. Soc. Pac. **121**, 993 (2009).

[104] H. Canovas, M. Rodenhuis, S. V. Jeffers, M. Min, and C. U. Keller, Data-reduction techniques for high-contrast imaging polarimetry, applications to ExPo, Astron. Astrophys. **531**, A102 (2011).

[105] A. J. Weitenbeck, Stars with ISM polarization observed with HPOL. III, Acta Astronomica **58**, 433 (2008).

[106] M. R. Meade, B. A. Whitney, B. L. Babler, K. H. Nordsieck, K. S. Bjorkman, and J. P. Wisniewski, HPOL: World's Largest Database of Optical Spectropolarimetry, AIP Conf. Proc. **1429**, 226 (2012).

[107] R. Siebenmorgen, N. V. Voshchinnikov, S. Bagnulo, N. L. J. Cox, J. Cami, and C. Peest, Large interstellar polarisation survey. II. UV/optical study of cloud-to-cloud variations of dust in the diffuse ISM, Astron. Astrophys. **611**, A5 (2018).

[108] S. Bagnulo, N. L. J. Cox, A. Cikota, R. Siebenmorgen, N. V. Voshchinnikov, F. Patat, K. T. Smith, J. V. Smoker, S. Taubenberger, L. Kaper *et al.*, Large interstellar polarisation survey (LIPS). I. FORS2 spectropolarimetry in the southern hemisphere, Astron. Astrophys. **608**, A146 (2017).

[109] F. Kislat, Constraints on Lorentz invariance violation from optical polarimetry of astrophysical objects, Symmetry **10**, 596 (2018).

[110] E. Angelakis, T. Hovatta, D. Blinov, V. Pavlidou, S. Kiehlmann, I. Myserlis, M. Böttcher, P. Mao, G. V. Panopoulou, I. Liodakis *et al.*, RoboPol: The optical polarization of gamma-ray-loud and gamma-ray-quiet blazars, Mon. Not. R. Astron. Soc. **463**, 3365 (2016).

[111] D. Hutsemékers, P. Hall, and D. Sluse, Optical linear polarization measurements of quasars obtained with the 3.6 m telescope at the La Silla observatory, Astron. Astrophys. **606**, A101 (2017).

[112] D. Blinov, V. Pavlidou, I. Papadakis, S. Kiehlmann, G. Panopoulou, I. Liodakis, O. G. King, E. Angelakis, M. Baloković, H. Das *et al.*, RoboPol: First season rotations of optical polarization plane in blazars, Mon. Not. R. Astron. Soc. **453**, 1669 (2015).